GEOSPHERE

GEOSPHERE; v. 13, no. 5

doi:10.1130/GES01414.1

20 figures; 3 tables; 2 supplemental files

CORRESPONDENCE: wmw4@cornell.edu

CITATION: White, W., Copeland, P., Gravatt, D.R., and Devine, J.D., 2017, Geochemistry and geochronology of Grenada and Union islands, Lesser Antilles: The case for mixing between two magma series generated from distinct sources: Geosphere, v. 13, no. 5, p. 1359–1391, doi:10.1130/GES01414.1.

Received 15 August 2016
Revision received 24 March 2017
Accepted 25 May 2017
Published online 27 July 2017

Geochemistry and geochronology of Grenada and Union islands, Lesser Antilles: The case for mixing between two magma series generated from distinct sources

William White[1], Peter Copeland[2], Daniel R. Gravatt[1,*], and Joseph D. Devine[3,†]

[1]Department of Earth and Atmospheric Science, Cornell University, Ithaca, New York 14853-1504, USA
[2]Department of Earth and Atmospheric Science, University of Houston, Houston, Texas 77204, USA
[3]Department of Geology, Brown University, Providence, Rhode Island 02912, USA

ABSTRACT

We report major-element, trace-element, and radiogenic-isotope analyses of 49 lavas and xenoliths as well as 35 $^{40}Ar/^{39}Ar$ ages from Grenada, Kick 'em Jenny submarine volcano, and several Grenadine Islands. Grenada magmas are compositionally unusual in several respects compared to other subduction-related magmas. Particularly controversial is the extent to which compositions reflect the presence of subducted sediment in their sources or assimilation of sediment in the arc crust and the relationship between two distinct Grenada magma series, the Sr-rich and ankaramitic C series and olivine-microphyric M series, erupted on the island. New $^{40}Ar/^{39}Ar$ ages show that eruption of these magmas has been interwoven both in time and space over the past 6 million years, during which the present volcanic edifice of Grenada has been built, indicating they share a common plumbing system. Consistent with earlier studies, our data show that the two series are isotopically distinct in their most mafic examples. At least 0.6% of a subducted sediment component must be added to depleted mantle to explain M-series isotopic compositions; considerably less, ~0.2%, subducted sediment is present in the C-series source. Trace elements and isotope ratios of both series are best modeled by the addition of slab-derived components predominantly through silicate melts, but the addition of hydrous fluids is also required, with the C series requiring a greater fluid component than the M series. This indicates the top of the slab is at or above its solidus beneath Grenada. C-series parental magmas are generated by significantly smaller peridotite melt fractions than M-series parents and may contain a fraction of pyroxenite melt as well.

Radiogenic-isotope ratios in C-series basalts correlate significantly with MgO, but oxygen-isotope ratios do not. This and other aspects of their evolution, including decreasing K_2O/Na_2O and Sr concentrations with decreasing MgO, cannot be explained by sediment assimilation previously proposed. Instead, these features are readily explained by mixing with evolved M-series magmas stored in the arc crust and, perhaps, assimilation of their crystallization products. Such mixing may also affect M-series magmas, but because M-series magmas constitute three-fourths of Grenada igneous products and because parent M-series magmas are notably more heterogeneous, the effects of this mixing are less obvious. Any assimilation of sediment within the arc crust has at best second-order effects of magma compositions.

The geochemistry of a pillow basalt from Mayreau Island is consistent with an earlier interpretation that the Grenadine Platform consists of uplifted oceanic crust formed through Eocene backarc spreading. Union Island consists of supra-subduction andesites and basalts (erupted between 6.5 and 3 million years ago) that are similar to those of Grenada. Kick 'em Jenny volcano is a distinct magma system from Grenada, but the neighboring volcanic islet of Isle de Caille is magmatically part of Grenada. A dacite dike cutting sedimentary rocks of the Tufton Hall Formation on Grenada yielded a $^{40}Ar/^{39}Ar$ age of 37.9 ± 0.2 Ma, suggesting the existence of supra-subduction volcanism in the region since the Eocene.

INTRODUCTION

The petrology and geochemistry of Grenada, the southernmost volcanic island of the Lesser Antilles island arc (Fig. 1), are unusual in several respects. First, many lavas are strongly incompatible-element enriched and have among the most radiogenic Sr and Pb and unradiogenic Nd- and Hf-isotope ratios of all intra-oceanic island-arc volcanics (IAV) (Hawkesworth and Powell, 1980; Thirlwall and Graham, 1984; Thirlwall et al., 1996; White and Dupré, 1986; White and Patchett, 1984). Second, the suite includes highly magnesian, primitive basalts, some of which contain peridotite xenoliths (Arculus, 1978), which are also unusual in an island-arc setting. Third, two distinct magma series occur. They were originally identified as a low-Sr and high-Sr series by Arculus (1976) and subsequently named the M and C series by Graham (1980) and Thirlwall and Graham (1984). The M series is distinguished by an abundance of olivine microphenocrysts in the more mafic members, while the C series is ankaramatic, with abundant large clinopyroxene phenocrysts in the more mafic lavas and is notably enriched in calcium and strontium. The two series are also

*Now at U.S. Environmental Protection Agency, Region 7, Lenexa, Kansas 66219, USA
†Deceased

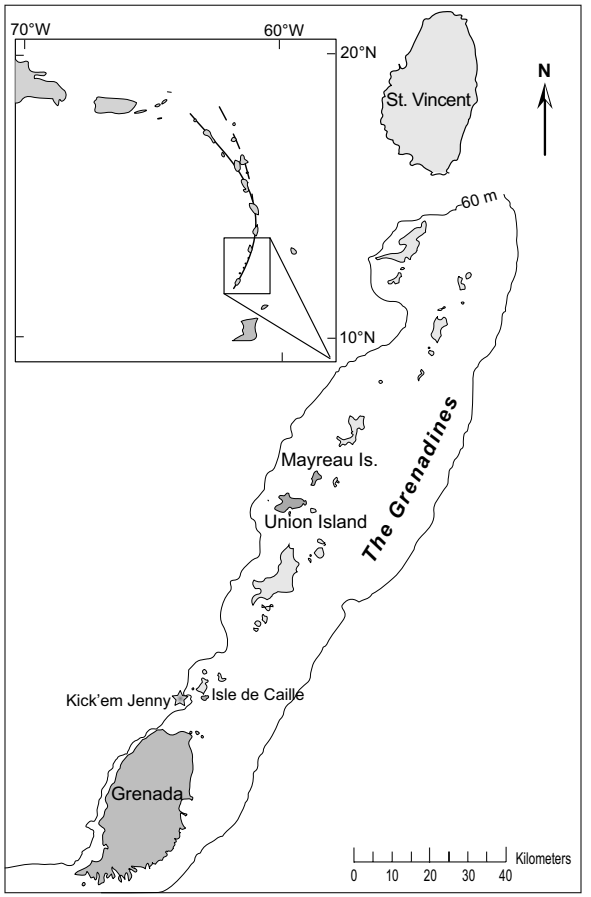

Figure 1. Map of Grenada and the Grenadines. Solid line follows the Neogene arc; the dashed line in inset follow the Paleogene arc. Islands included in this study—Grenada, Isle de Caille, Union, and Mayreau—are shown in a darker shade. Also shown is the location of Kick 'em Jenny submarine volcano.

distinguishable, at least in the more mafic examples, by their Sr, Nd, and Pb isotopic compositions (Hawkesworth and Powell, 1980; Thirlwall and Graham, 1984; Thirlwall et al., 1996), with the M series having the more enriched isotopic signatures. Fourth, many of the more mafic members of both the C and M series are nepheline-normative alkali basalts, some strongly so (Arculus, 1976; Sigurdsson et al., 1973), which is also highly unusual for subduction-related magmas, which are almost exclusively calc-alkaline or tholeiitic. Both series nevertheless evolve to quartz-normative andesitic and dacitic compositions more typical of IAV.

Controversy surrounds the interpretation of several aspects of Grenadian volcanism. First, how old is the island? Potassium-argon ages from Grenada reported by Briden et al. (1979) ranged from 0.94 Ma to 21.4 Ma. However, Speed et al. (1993) obtained $^{40}Ar/^{39}Ar$ plateau ages of 1.34–1.79 Ma from the same andesite that Briden et al. (1979) dated at 21.2 Ma, suggesting Grenada was far younger; but no additional $^{40}Ar/^{39}Ar$ ages have been reported to test this. Second, White and Dupré (1986) and Carpentier et al. (2008) pointed out that the enriched isotopic signatures in Grenadian magmas were a consequence of South American–derived sediment with particularly enriched isotopic signatures being subducted beneath the arc and contributing to the magma source. On the other hand, Thirlwall and Graham (1984) found correlations between isotope ratios and major elements in Grenadian lavas that suggested sediment assimilation accompanied fractional crystallization. Subsequently, Thirlwall et al. (1996) found that O-isotope ratios in clinopyroxene of C-series lavas correlated with radiogenic-isotope ratios, which they argued provided further evidence of assimilation-fractional crystallization (AFC). Although Thirlwall et al. (1996) did not argue this accounted entirely for the extreme isotopic compositions on Grenada, Bezard et al. (2014), extrapolating from a study of St. Lucia, where even more extreme compositions occur, took a more extreme view, stating, "assimilation seems to be responsible not only for the isotopic heterogeneity observed in St. Lucia but also in the whole Lesser Antilles" (p. 51). Third, Thirlwall et al. (1996) concluded that the M and C series are derived from distinct mantle sources, with the parental magmas of the C series, which are not seen at the surface, having been produced by melting of a less incompatible-enriched mantle source. In contrast, Stamper et al. (2014b) concluded based on experiments that "the geochemically and petrographically distinct M- and C-series lavas on the island can be produced from hydrous melting of a common picritic source" (p. 1), with the compositional differences resulting from the M series having undergone differentiation in the uppermost mantle at 1.4–1.8 GPa, while the C series differentiated in the shallow crust at ~0.2 GPa.

The questions raised in these controversies are central to our understanding of subduction-related volcanism, particularly in the Lesser Antilles. If Grenada is actually 20 million years old, it implies quite low magma production rates; younger ages would imply higher magma production rates. Subducted sediments are widely believed to be an important contributor to island-arc magma sources (e.g., Plank, 2016), and subduction-related volcanism is similarly widely believed to be an important mechanism of continental crust generation (e.g., Taylor and McLennan, 1985). Lesser Antilles crust is more similar to continental crust both compositionally and seismically than most arcs (Gazel et al., 2015). If sediment assimilation rather than sediment subduction accounts for the isotopic compositions of Lesser Antilles magmas, paradigms about subduction zone processes and their role in crust-mantle evolution must be re-examined. And can fractional crystallization alone account for composition as distinct as those of the C and M series? If not, why do such distinct magma compositions appear on Grenada?

Additional key questions relate to the Grenadines, a series of low-lying islands located between Grenada and the next major island to the north,

St. Vincent (Fig. 1). What is the nature of volcanism and its timing? Are the magmas similar to those in Grenada or similar to more typical island-arc volcanism occurring on St. Vincent to the north? Do the basalts of Mayreau Island (Fig. 1; see description below) have geochemical signatures of convergent boundary volcanism, or do they have divergent boundary (mid-ocean ridge or backarc) signatures as predicted by Speed et al. (1993)?

To address these and related questions, we undertook a major geochronological and geochemical study of Grenada and some of the Grenadine Islands. We report major-element, trace-element, and radiogenic-isotope analyses on 49 samples from Grenada, Isle de Caille, Kick 'em Jenny, and Union and Mayreau islands as well as 35 $^{40}Ar/^{39}Ar$ ages from Grenada and Union. Our results show that the exposed volcanic edifice on Grenada is young, mostly less than 6 million years old. In contrast to earlier work, we find that magma mixing, possibly combined with assimilation of the igneous rocks in the arc crust rather than sediment assimilation, explains correlations between trace elements, major elements, and isotope ratios.

GEOLOGIC BACKGROUND

The Lesser Antilles island arc has formed in response to the slow (~2 cm/yr) subduction of the westward-moving South American plate beneath the Caribbean plate (Fig. 1). The arc pivoted westward in the Miocene, leaving a string of extinct volcanic islands (the "Limestone Caribbees") east of the modern arc in the north, while the modern Neogene and Paleogene arcs overlap south of Guadaloupe (Nagle et al., 1976) (Fig. 1, inset). The southern Lesser Antilles volcanoes lie ~140 km above the Benioff Zone, which dips at an average of 42° (Syracuse et al., 2010). Grenada consists mainly of basaltic volcanic rocks, although andesite and rare dacites are also present. As noted earlier, these can be divided into two quite distinct magma series, the M series and the less common C series. M-series basalt lava flows are not notably vesicle rich, but the textures of M-series basaltic blocks produced by recent explosive eruptions are scoriaceous, suggesting the magmas are water rich. C-series lava flows are only rarely observed. More typically, C-series rocks are found in fields of more or less massive boulders (<2 m diameter) or as stream valley fill, making it difficult to readily infer eruption styles, but a lack of vesicles suggests lower water content. Turbiditic and hemipelagic sedimentary rocks, the Tufton Hall Formation, also outcrop in several localities in Grenada (Fig. 1). These rocks are of Eocene age based on the foraminiferal fauna (Speed et al., 1993).

Although no historical eruptions have occurred on Grenada, Kick 'em Jenny submarine volcano, which is located just 7 km north of Grenada and has grown to within 187 m of sea level, has erupted repeatedly since 1939, most recently in July 2015 (Global Volcanism Program, 2015). Also, lava flows on the small islet of Isle de Caille, located just a few kilometers east of Kick 'em Jenny, appear to be less than ~1000 years old based on their partially unvegetated nature and ^{226}Ra excesses (Turner et al., 2001). Although potassium-argon ages from Grenada reported by Briden et al. (1979) ranged from 0.94 Ma to 21.4 Ma, as noted earlier, Speed et al. (1993) obtained $^{40}Ar/^{39}Ar$ plateau ages of 1.34–1.79 Ma from one of these samples.

The Grenadines are a series of low-lying islands between Grenada and the next major volcanic island to the north, St. Vincent. The islands consist primarily of Neogene subduction-related basalts and andesites but also have outcrops of Oligocene and Eocene sedimentary and magmatic rocks. Some of the oldest rocks are found on Mayreau Island, which is located roughly half way between Grenada and St. Vincent and offset somewhat to the west of the main arc and neighboring Grenadines. These include pillow basalts overlain by Eocene pelagic limestones that are overlain and intruded by Neogene volcanics. On the bases of major- and minor-element and rare-earth compositions of whole rocks and of clinopyroxene phenocryst compositions, Speed and Walker (1991) interpreted the pillow basalts as having been produced by middle Eocene backarc spreading. The $^{40}Ar/^{39}Ar$ ages of two Mayreau basalts obtained by Speed et al. (1993) are, however, younger at 14.1 ± 0.8 Ma and 12.4 ± 1.8 Ma, which Speed et al. (1993) interpret as having been reset by intruding Neogene dikes. According to Speed et al. (1993), the southern Lesser Antilles arc platform formed as an uplift of this backarc crust and associated sedimentary rocks in an east-tilted half horst during the Miocene. It is upon this backarc crust that the Neogene arc volcanics of Grenada and the Grenadines were later erupted. The trace-element data upon which Speed and Walker (1991) based this interpretation, were, however, obtained by atomic emission spectrometry and X-ray fluorescence (XRF), and many key elements were near or below detection limit; therefore, further investigation seems justified.

Union Island, located ~6 km south of Mayreau, is also offset to the west of neighboring Grenadines. It consists mainly of Neogene volcanic rocks younger than 7 Ma, based on K-Ar dating of Briden et al. (1979) and Westercamp et al. (1985). However, an outcrop of Eocene sandstone chert and intrusive and extrusive igneous rocks occurs in fault contact with the Neogene volcanics (Speed et al., 1993).

METHODS

Sample descriptions and locations are listed in Supplemental Table S1[1]. Figure 2 shows the locations of the Grenada samples.

Geochronology

Twenty-nine samples from Grenada and six samples from Union have been analyzed by $^{40}Ar/^{39}Ar$ methods at the University of Houston. Large basalt samples were crushed, and groundmass particles were handpicked from the 60–100 mesh fraction. Care was taken to avoid any phenocrysts of olivine, pyroxene, or plagioclase, but microcrysts of probably mostly plagioclase were certainly present in the analyzed samples. Nevertheless, the groundmass is likely the most potassic phase in these rocks and least likely to have problems

Supplementary Table S1. Sample locations and descriptions

Sample	Latitude °N	Longitude °W	Location	Description
GDA004	12.212	61.697	S of Crayfish Bay	M series andesitic block and ash flow
GDA005	12.225	61.608	Levera Bay shoreline	C series basalt cobble
GDA008	12.062	61.755	Queen's Park quarry scoria cone	M Series basaltic scoria which bears harzburgite nodules
GDA011	12.125	61.625	Pilot Hill quarry, Grenville	M Series Basaltic scoria, mostly < 1 cm
GDA021	12.032	61.722	River ford, Hope Vale Estate	M Series basalt cobble
GDA031	12.128	61.733	Mon Plaisir	C series cobble from ravine cut in large lava flow
GDA033	12.133	61.746	Grand Roy bridge	Amphibole-bearing crustal xenolith
GDA034	12.198	61.705	N end of Victoria	C series basaltic lava flow fragment
GDA035	12.210	61.672	Duquesne	C-series basaltic lava flow fragment
GDA037	12.2283	61.618	W end of Levera Bay	Tufton Hall Formation; near location of sample GR64 of Westercamp et al. (1985).
GDA038	12.227	61.628	NNW of Levera Hill	C-series basalt boulder field
GDA040	12.188	61.653	Mt. Craven	M Series hornblende andesite
GDA043	12.189	61.650	High Cliff Point	assorted hornfels/amphibolite xenoliths
GDA045	12.188	61.188	Montreuil Estate, road heading west, up the hill from the village	M Series vitrophyric (in thin section) basaltic tephra fall
GDA049	12.207	61.612	S of Bathway Beach, Grenada Bay	C-series boulder
GDA063B	12.023	61.777	Quarantine	M Series basalt flow
GDA077	12.093	61.759	N shore of Flamingo Bay	M Series fine-grained basalt
GDA080	12.133	61.746	Grand Roy, scarp by bridge	scoria with hbl-cpx xenolith
GDA084B	12.088	61.72	Annandale Falls	M Series M-series basalt boulder from stream bed below falls
GDA086	12.205	61.672	Union village	Tufton Hall Formation
GDA091	12.147	61.737	Dothan, roadside sea scarp	Xenoliths: Ol & chromite pods in coarse Hble + Cpx matrix

[1]Supplemental Table S1. Sample locations and descriptions. Please visit http://doi.org/10.1130/GES01414.S1 or the full-text article on www.gsapubs.org to view Supplemental Table S1.

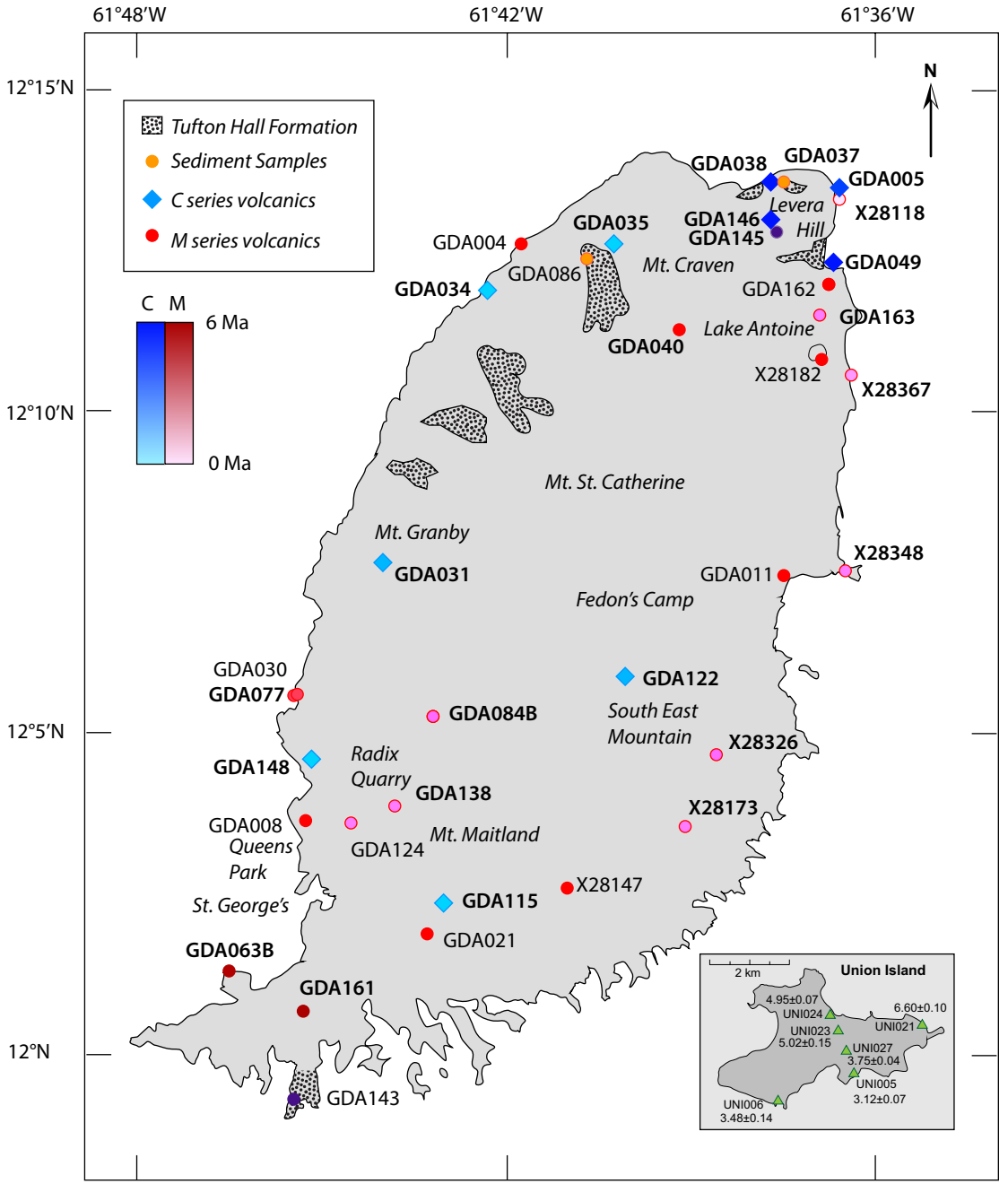

Figure 2. Location of Grenada samples analyzed in this study. C-series samples are shown as blue shaded diamonds; M-series samples are depicted by red circles. Names of major volcanic centers are shown. Color intensity is scaled to age of Grenada samples: darker shades correspond to older ages. $^{40}Ar/^{39}Ar$ ages (Ma). Inset shows the locations of samples from Union Island.

with "excess Ar" sometimes observed with analysis of olivine, pyroxene, and plagioclase feldspar. Because of the youth and composition of these samples, a minimum of 48 mg was analyzed, with the mass of most samples in excess of 100 mg (Supplemental Table S1 [see footnote 1]). Samples were wrapped in Sn foil along with similarly wrapped samples of Fish Canyon Tuff (FCT) sanidine as fluence monitor. Samples were placed in quartz tubes with standards every ~15–20 mm.

Samples were irradiated at the Ford Nuclear Reactor at the University of Michigan in four separate irradiations. Interfering reactions on Ca and K were monitored using a zero-age, high-K synthetic glass and optical-grade CaF_2. The correction factors for each sample are listed in Supplemental Table S1 (see footnote 1) along with the daily discrimination and sensitivity of the mass spectrometer.

Fluence monitors were heated as single crystals loaded into a copper disc and heated using a 10 W CO_2 laser. Up to five sanidines were analyzed, and the associated *J* factors were averaged to characterize that location. *J* factors of unknowns were calculated by interpolation between standards. In all of these samples, analytical uncertainty is much larger than the uncertainty in *J*. All ages in this report are calculated assuming an age of 28.20 Ma for FCT sanidine (Kuiper et al., 2008).

Unknown samples were step-heated in a double-vacuum resistance furnace. Temperature was monitored by a thermocouple placed in a well on the outside of the Mo crucible. The distance from the thermocouple to the samples was ~1–2 cm. Because of the large size and potential complications coming from fluid inclusions, zeolites, or other sources of water and CO_2, these samples were gettered using a SAES GP50 getter for 1000 seconds.

Argon evolved from both standards and unknowns was analyzed on a MAP-215 rare-gas mass spectrometer in static mode using the electron multiplier. Five cycles of the five Ar isotopes were analyzed, and the value of each nuclide was determined by extrapolation back to time zero.

Uncertainty in the age reported in Table 1 includes propagation of all uncertainties of time zero extrapolation, *J* factor, and correction factors (not shown in the table). For analysts interested in the problems of dating low-K young basalts, we note that in early attempts at dating Grenadian basalts, we sent only 40 mg of material to the reactor and we gettered for only 300 seconds; these attempts did not yield satisfactory results.

Geochemistry

Major elements for many of the samples with designations beginning with GDA or KEJ analyzed in this study were previously reported by Devine (1995) or Devine and Sigurdsson (1995). Major-element data for sample numbers beginning with "X" or WIC are from (Brown et al., 1977). As pointed out by Thirlwall and Graham (1984), these data have systematic errors, and we have corrected them using correction factors given in Devine (1995). New major-element data presented here were determined by XRF using a Fisons/ARL 8410 XRF spectrometer at Syracuse University. Powdered samples were mixed with a lithium tetraborate flux in a 1:9 ratio and fused into a glass disk. These disks were then placed in the XRF spectrometer and analyzed according to the procedures outlined in Coler et al. (1997). Judging from analysis of U.S. Geological Survey (USGS) standards BCR-2, AGV-1, and BHVO-1, reproducibility ranged from 0.8% for the least abundant elements to better than 0.2% for the most abundant elements (±1 sigma) with accuracy better than 1%.

Trace-element concentrations were determined at Cornell University using a Fisons/VG PlasmaQuad 2+ inductively coupled plasma mass spectrometer (ICP-MS). Samples were powdered in a boron carbide mortar and pestle, and 100 mg portions were digested in 3 ml HF and 6 ml HNO_3 in cleaned Teflon Savillex capsules. The dissolved sample was dried and redissolved in HNO_3 and water to achieve a dilution factor of 1000 and a final nitric concentration of less than 1%. This solution was introduced into the ICP-MS, and elemental abundances were determined by scanning several mass ranges (e.g., ^{85}Rb to ^{93}Nb, ^{136}Ba to ^{181}Ta) in different analysis "runs." The raw data were then blank corrected, reduced, and corrected using the Excel macro described in Cheatham et al. (1993). This procedure uses data from identical solutions interspersed with the unknown samples at regular intervals within a batch to calculate a nonlinear function that represents spectrometer drift with time. The macro then applies this function to the data on the unknowns and corrects their abundances based on the spectrometer's sensitivity at the time each unknown was analyzed. Data reported here are means of three or more replicate analyses of each solution performed on different days. Based on replicate analyses of standards, precision exceeded 5% for all elements.

Lead-, Sr-, and Nd-isotope ratios were determined using a Fisons/VG Sector 54 thermal ionization mass spectrometer at Cornell University. Sample chips were prepared using a steel chisel and Plattner mortar and then cleaned ultrasonically in HCl to remove surface contamination. The chips (250 mg, typically) were digested in HF and HBr in cleaned Teflon Savillex capsules and dried. The sample was then taken up in 3 ml 0.5N HBr and centrifuged, and the supernatant was loaded onto a column of Dowex AG1x8 anion resin. After eluting all other ions with 0.5N HBr, Pb was eluted with 2.0N HCl, dried, and then re-loaded onto a fresh column of AG1x8, and the entire separation repeated to insure a clean separation of Pb. Lead blanks, as measured by isotope dilution, were typically ~60 pg.

Centrifuged solids from the Pb digestion, as well as the washes from the Pb elution, were combined, HCl was added, and the mixture was dried; $HClO_4$ was added, and the sample was again dried down. The sample was taken up in 2.5N HCl, a 50 mg rock equivalent volume was loaded onto a column of ~5 ml Dowex AG50wx12 resin, and the Sr was eluted with 2.5N HCl. The split containing the rare-earth element (REE) was collected from this column in 6N HCl, dried, taken up in 0.14N HCl, loaded onto a column of Di-(2-ethylhexyl)phosphoric acid-coated Teflon beads, and Nd eluted with 0.14N HCl.

Lead samples were loaded on degassed rhenium filaments on a bed of silica gel and run in a static collector mode. Mass fractionation was monitored and corrected for by concurrently loading and running multiple beads

TABLE 1. SUMMARY OF $^{40}Ar/^{39}Ar$ AGES

Sample	Location	Material	Plateau age (Ma) (±1σ)	Gas on plateau (%)
Grenada C series				
GDA005	Levera Bay	Groundmass	4.77 ± 0.11	96.0
GDA031	Queen's Park	Groundmass	0.87 ± 0.03	66.7
GDA034	Victoria	Groundmass	0.59 ± 0.03	83.2
GDA035	Victoria	Groundmass	0.55 ± 0.02	89.5
GDA038	Levera Bay	Groundmass	5.51 ± 0.07	97.2
GDA049	Grenada Bay	Groundmass	5.18 ± 0.06	84.3
GDA115	Mon Delice	Groundmass	1.30 ± 0.03	78.5
GDA122	Petit Balthazar	Groundmass	0.94 ± 0.06	95.9
GDA146	Levera Hill	Groundmass	5.83 ± 0.09	96.1
Grenada M series				
GDA021	Hope Vale	Groundmass	1.70 ± 0.05	73.8
GDA045	Monteuil Estate	Whole rock	0.06 ± 0.08	100
GDA063B	Quarantine	Groundmass	4.18 ± 0.09	86.3
GDA077	Flamingo Bay	Groundmass	1.40 ± 0.04	79.5
GDA084B	Annandale Falls	Groundmass	0.86 ± 0.06	99.6
GDA124	Mount Gay	Groundmass	0.52 ± 0.14	79.8
GDA138	Radix cone	Groundmass	0.59 ± 0.14	98.6
GDA143a	Prickly Point	Groundmass	37.60 ± 0.62	100
GDA143b	Prickly Point	Groundmass	38.41 ± 0.23	100
GDA143		*Weighted average*	*38.31 ± 0.22*	
GDA145	Levera Hill	Groundmass	6.06 ± 0.06	98.3
GDA148	Grand Mal	Groundmass	1.90 ± 0.03	77.0
GDA159A	Providence	Amphibole	0.72 ± 0.16	68.4
GDA161a	Lance aux Espines	Groundmass	4.35 ± 0.30	98.2
GDA161b	Lance aux Espines	Groundmass	4.62 ± 0.04	100
GDA161		*Weighted average*	*4.62 ± 0.04*	
GDA162	Riviere Sallee	Groundmass	2.74 ± 0.42	100
GDA163	Riviere Sallee	Groundmass	0.52 ± 0.03	63.6
X28118	Bedford Point	Groundmass	0.30 ± 0.50	84
X28173	Crochu	Groundmass	0.64 ± 0.04	100
X28182	Lake Antoine	Groundmass	1.82 ± 0.30	74.9
X28326	St. Francis River	Groundmass	0.90 ± 0.05	72.2
X28348	Telescope Point	Groundmass	0.54 ± 0.11	94.4
X28367	Peggy's Whim	Groundmass	0.35 ± 0.03	74.2
Union Island				
UNI005	Clifton Reserve	Groundmass	3.12 ± 0.07	92.3
UNI006	Miss Cambell	Groundmass	3.84 ± 0.04	96.3
UNI021	East of Fort Hill	Groundmass	6.60 ± 0.10	92.3
UNI023	North of Pinnacle	Groundmass	5.02 ± 0.15	85.9
UNI024	Bloody Head	Groundmass	4.95 ± 0.07	93.2
UNI027	Radio Station	Groundmass	3.75 ± 0.04	94.2

of NBS-981 Pb standard with each sample batch and applying a fractionation correction to the unknown ratios based on the deviation of the standards from their accepted values, which were assumed to be $^{206}Pb/^{204}Pb$ = 16.940, $^{207}Pb/^{204}Pb$ = 15.493, $^{208}Pb/^{204}Pb$ = 37.722 (Galer and Abouchami, 1998). The average measured values for NSB981 were $^{206}Pb/^{204}Pb$ = 16.894 ± 0.012, $^{207}Pb/^{204}Pb$ = 15.435 ± 0.014, $^{208}Pb/^{204}Pb$ = 37.531 ± 0.038 (2σ). Strontium samples were loaded in HCl on degassed tungsten filaments on a bed of $TaCl_5$ and run in the Sector 54 using a procedure with three collector cups. An exponential correction factor was applied based on a value of the $^{86}Sr/^{88}Sr$ equal to 0.11940. The average of all NBS-987 Sr standards analyzed during this period was 0.710258 ± 0.000015 (±2σ). Neodymium samples were loaded on degassed rhenium filaments on a bed of Dowex AG1x8 anion resin beads (which serves as a reductant to inhibit NdO^+ formation) with phosphoric acid and run using a 7-cup procedure. An exponential correction factor was applied based on a value of the $^{146}Nd/^{144}Nd$ ratio equal to 0.7219. The average of Ames Nd standards analyzed during this period was 0.512138 ± 0.000006 (±2σ). These 2σ values represent our best estimate of the reproducibility of our analyses; in-run statistics were better.

RESULTS

Petrography

Petrographic observations on the M series were reported in Devine (1995). Here we focus on the C series. The most striking feature of C-series basalts is the relative abundance of large (~1 cm), euhedral clinopyroxene (cpx) phenocrysts. The strongly porphyritic textures of C-series basalts contrast with the fine-grained textures of M-series basalts. Olivine is always subordinate to cpx in size and abundance in the C series, whereas the reverse is true of primitive members of the M-series rocks.

Plagioclase is typically confined to the groundmass in C-series basalts, where it may coexist with magnetite, phlogopite, or other accessory phases, or be rimmed by alkali feldspar. Sector zoning and very fine oscillatory zoning of cpx phenocrysts are common features in C-series basalts, in contrast to clinopyroxenes in basalts of the northern Lesser Antilles (Arculus, 1978). The pyroxenes of C-series basalts are also apt to be rich in irregularly shaped inclusions filled by zeolite minerals that may be alteration products of what were once glassy melt inclusions. Oxides of the spinel-hercynite solid solution series (pleonaste) are also included in cpx phenocrysts, as are other rare, exotic oxides. None of these inclusion assemblages is observed in clinopyroxenes from M-series basalts.

$^{40}Ar/^{39}Ar$ Geochronology

Twenty-nine Grenada samples, ten from the C series and 19 from the M series, were dated by $^{40}Ar/^{39}Ar$ (one sample, GDA161, was analyzed in duplicate); the detailed analytical data are given in Supplemental Table S2[2] and summarized in Table 1, and ages of Grenadian samples are coded by color intensity in Figure 2. Ages of Union Island samples are also shown in Figure 2. All of these samples give relatively simple "plateaus," ranging from 64% to 99% of the ^{39}Ar released; release spectra for the M-series basalts are shown in Figure 3; release spectra for the C-series basalts are shown in Figure 4; release spectra for basalts from Union are shown in Figure 5; release spectra for a dacite dike from southernmost Grenada are shown in Figure 6. With the exception of this dike, GDA143, which is discussed below, ages range from 6.06 to 0.06 Ma. Figure 7A compares $^{40}Ar/^{39}Ar$ ages to the K-Ar ages from Briden et al. (1979) for samples we judge to be comparable; the 21.2 Ma K-Ar age reported by Briden et al. (1979) on a sample from the Northern Domes is likely in error, probably due to inherited argon. A number of our Northern Domes samples are older (4.8–6.1 Ma) than the 1.9–2.3 Ma $^{40}Ar/^{39}Ar$ ages reported by Speed et al. (1993), but much younger lavas are found in this area as well. Lavas older than 4 Ma are also found in the south of the island (GDA063 and GDA061). Other than a possible clustering of the oldest ages in the north and south, there is no apparent relationship between age and location, and lavas younger than 1 Ma occur throughout the island. Overall, our results are consistent with the relative young age of the volcanic edifice of Grenada inferred by Speed et al. (1993).

Figure 7B shows the distribution of ages in time for both Grenada and Union Island (the two Isle de Caille samples are included in the distribution with assumed ages of 0.001 Ma). Ages of Grenada samples tend to cluster between 0 and 2 Ma and between 4 and 6 Ma: only a single sample, GDA162, has an age between 2 and 4 Ma. Significantly, this clustering is true of both the C and the M series, although the paucity of ages between 2 and 4 Ma may represent a preservation or sampling bias. Thus, eruption of C- and M-series lavas shows the same distribution in both space and time (Fig. 2). Interestingly, it appears that volcanism may have been most recently active on Union Island just during this period of apparent inactivity on Grenada. The other major period of activity on Union Island was before 5 Ma.

The one much older sample, GDA143, is a dacite dike that intrudes an outcrop of Tufton Hall Formation at Prickly Point at the southernmost tip of the island. Two analyses of this sample give plateaus corresponding to ages of 37.2 ± 0.6 and 38.0 ± 0.2 Ma (Fig. 6) with a weighted average age of 37.9 ± 0.2 Ma. Speed et al. (1993) reported the Tufton Hall Formation outcrops contain planktonic foraminifera from biostratigraphic zone P16. Berggren and Pearson (2005) place the base of zone P16 at ca. 35.2 Ma. Our age suggests the Tufton Hall must be older than 37.7 Ma. However, the Tufton Hall outcrops examined by Speed et al. (1993) are all in the northern part of the island. Thus, either the Tufton Hall Formation at the southern part of the island is at least 2.5 million years older than outcrops in the north, or the Eocene foraminiferal chronostratigraphy needs to be reconsidered.

Geochemistry

Major-element results are listed in Table 2; trace-element concentrations and isotope ratios are given in Table 3. Many of the basalts are nepheline normative. The most mafic examples of the C series are uniformly nepheline

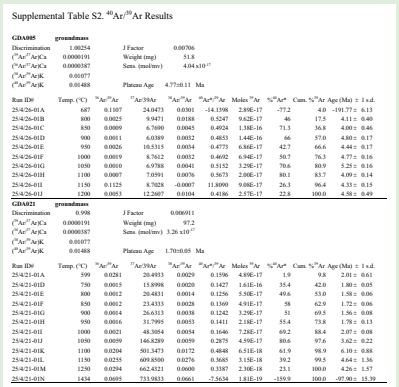

Supplemental Table S2. $^{40}Ar/^{39}Ar$ Results

GDA105	groundmass									
Discrimination	1.00254		J Factor	0.00706						
$(^{37}Ar/^{39}Ar)Ca$	0.0000191		Weight (mg)	51.8						
$(^{36}Ar/^{37}Ar)Ca$	0.0000387		Sens. (mol/mv)	4.04 x10^{-17}						
$(^{40}Ar/^{39}Ar)K$	0.01077									
$(^{38}Ar/^{39}Ar)K$	0.01488		Plateau Age	4.77±0.11 Ma						
Run ID#	Temp. (°C)	$^{40}Ar/^{39}Ar$	$^{37}Ar/^{39}Ar$	$^{38}Ar/^{39}Ar$	$^{40}Ar^{*}/^{39}Ar$	Moles ^{39}Ar	$\%^{40}Ar^{*}$	Cum. $\%^{39}Ar$	Age (Ma) ± 1 s.d.	
25/4/26-01A	687	0.1107	24.0473	0.0301	-14.1398	2.89E-17	-77.2	4.0	-191.77 ± 6.13	
25/4/26-01B	800	0.0025	9.9471	0.0188	0.3247	9.62E-17	46	17.5	4.11 ± 0.40	
25/4/26-01C	850	0.0089	6.7690	0.0045	0.4924	1.38E-16	71.3	36.8	4.00 ± 0.46	
25/4/26-01D	900	0.0011	6.0389	0.0032	0.4853	1.44E-16	66	57.0	4.80 ± 0.17	
25/4/26-01E	950	0.0026	10.5315	0.0034	0.4773	6.86E-17	42.7	66.6	4.44 ± 0.17	
25/4/26-01F	1000	0.0019	8.7612	0.0032	0.4692	6.94E-17	50.7	76.3	4.77 ± 0.16	
25/4/26-01G	1050	0.0010	6.9788	0.0041	0.5152	3.29E-17	70.6	80.9	5.25 ± 0.16	
25/4/26-01H	1100	0.0007	7.0591	0.0076	0.5673	2.00E-17	80.1	83.7	4.09 ± 0.14	
25/4/26-01I	1150	0.1123	8.7028	-0.0007	11.8090	9.08E-17	26.3	96.4	4.33 ± 0.15	
25/4/26-01J	1200	0.0053	12.2607	0.0104	0.4186	2.57E-17	22.8	100.0	4.58 ± 0.49	
GDA021	groundmass									
Discrimination	0.998		J Factor	0.006911						
$(^{37}Ar/^{39}Ar)Ca$	0.0000191		Weight (mg)	97.2						
$(^{36}Ar/^{37}Ar)Ca$	0.0000387		Sens. (mol/mv)	3.26 x10^{-17}						
$(^{40}Ar/^{39}Ar)K$	0.01077									
$(^{38}Ar/^{39}Ar)K$	0.01488		Plateau Age	1.70±0.05 Ma						
Run ID#	Temp. (°C)	$^{40}Ar/^{39}Ar$	$^{37}Ar/^{39}Ar$	$^{38}Ar/^{39}Ar$	$^{40}Ar^{*}/^{39}Ar$	Moles ^{39}Ar	$\%^{40}Ar^{*}$	Cum. $\%^{39}Ar$	Age (Ma) ± 1 s.d.	
25/4/21-01A	599	0.0281	20.4933	0.0029	0.1596	4.89E-17	1.9	9.8	2.01 ± 0.61	
25/4/21-01D	750	0.0015	15.8998	0.0020	0.1427	1.61E-16	33.4	42.0	1.80 ± 0.05	
25/4/21-01E	800	0.0012	20.4831	0.0014	0.1256	5.50E-17	49.6	53.0	1.58 ± 0.06	
25/4/21-01F	850	0.0012	23.4333	0.0028	0.1369	4.91E-17	58	62.9	1.72 ± 0.06	
25/4/21-01G	900	0.0014	26.6313	0.0038	0.1242	3.29E-17	51	69.5	1.56 ± 0.08	
25/4/21-01H	950	0.0016	31.7995	0.0053	0.1411	2.18E-17	55.4	73.8	1.78 ± 0.13	
25/4/21-01I	1000	0.0021	48.3054	0.0054	0.1646	7.28E-17	69.2	88.4	2.07 ± 0.08	
25/4/21-01J	1050	0.0059	146.8289	0.0059	0.2875	4.59E-17	80.6	97.6	3.62 ± 0.22	
25/4/21-01K	1100	0.0204	501.3473	0.0172	0.4848	6.51E-18	61.9	98.9	6.10 ± 0.88	
25/4/21-01L	1150	0.0255	609.8500	0.0276	0.3685	3.15E-18	39.2	99.5	4.64 ± 1.36	
25/4/21-01M	1250	0.0294	662.4321	0.0600	0.3387	2.39E-18	23.1	100.0	4.26 ± 1.57	
25/4/21-01N	1434	0.0695	733.9833	0.0661	-7.5634	1.81E-19	-159.9	100.0	-97.90 ± 15.39	

[2]Supplemental Table S2. $^{40}Ar/^{39}Ar$ results. Please visit http://doi.org/10.1130/GES01414.S2 or the full-text article on www.gsapubs.org to view Supplemental Table S2.

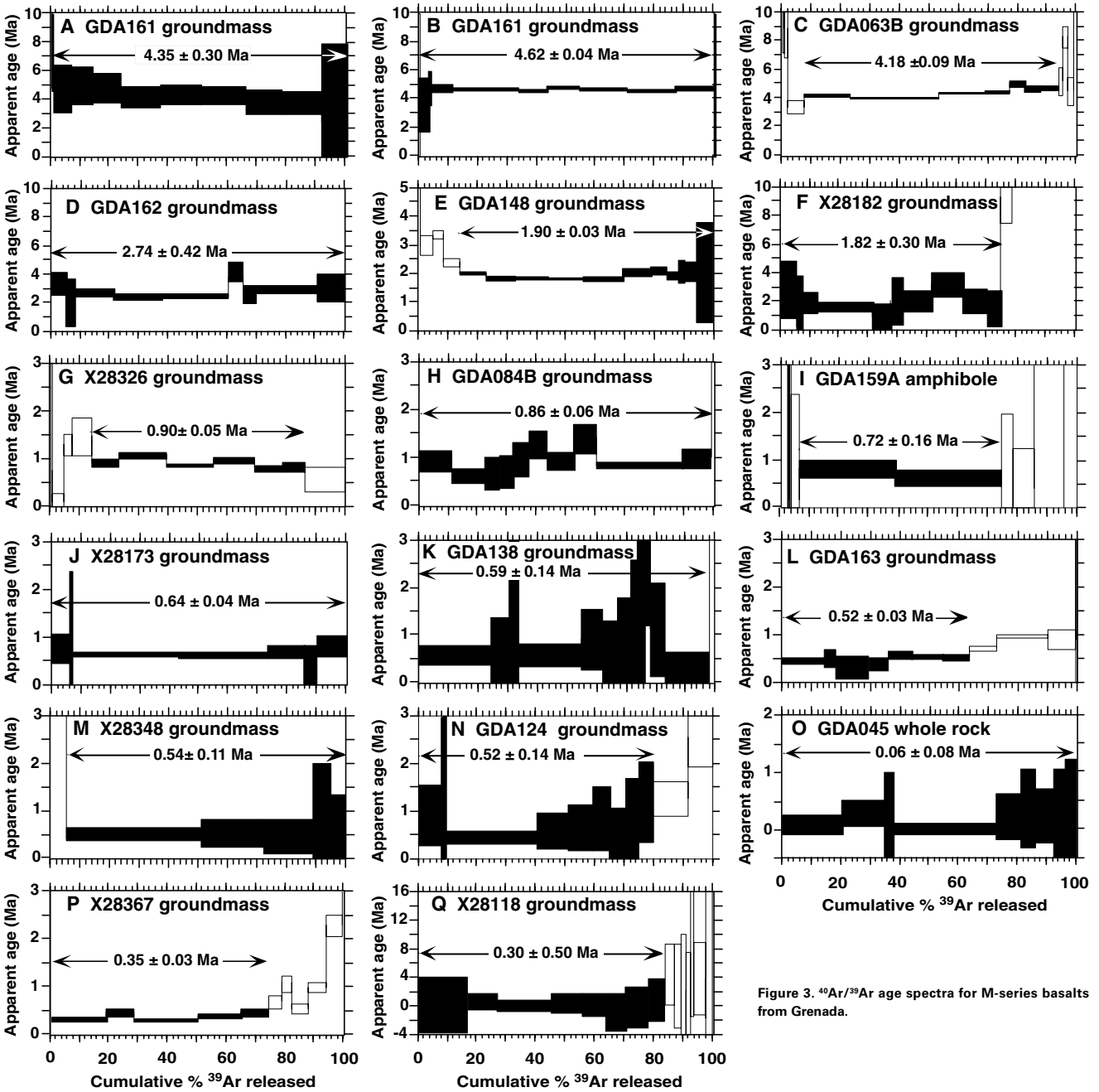

Figure 3. $^{40}Ar/^{39}Ar$ age spectra for M-series basalts from Grenada.

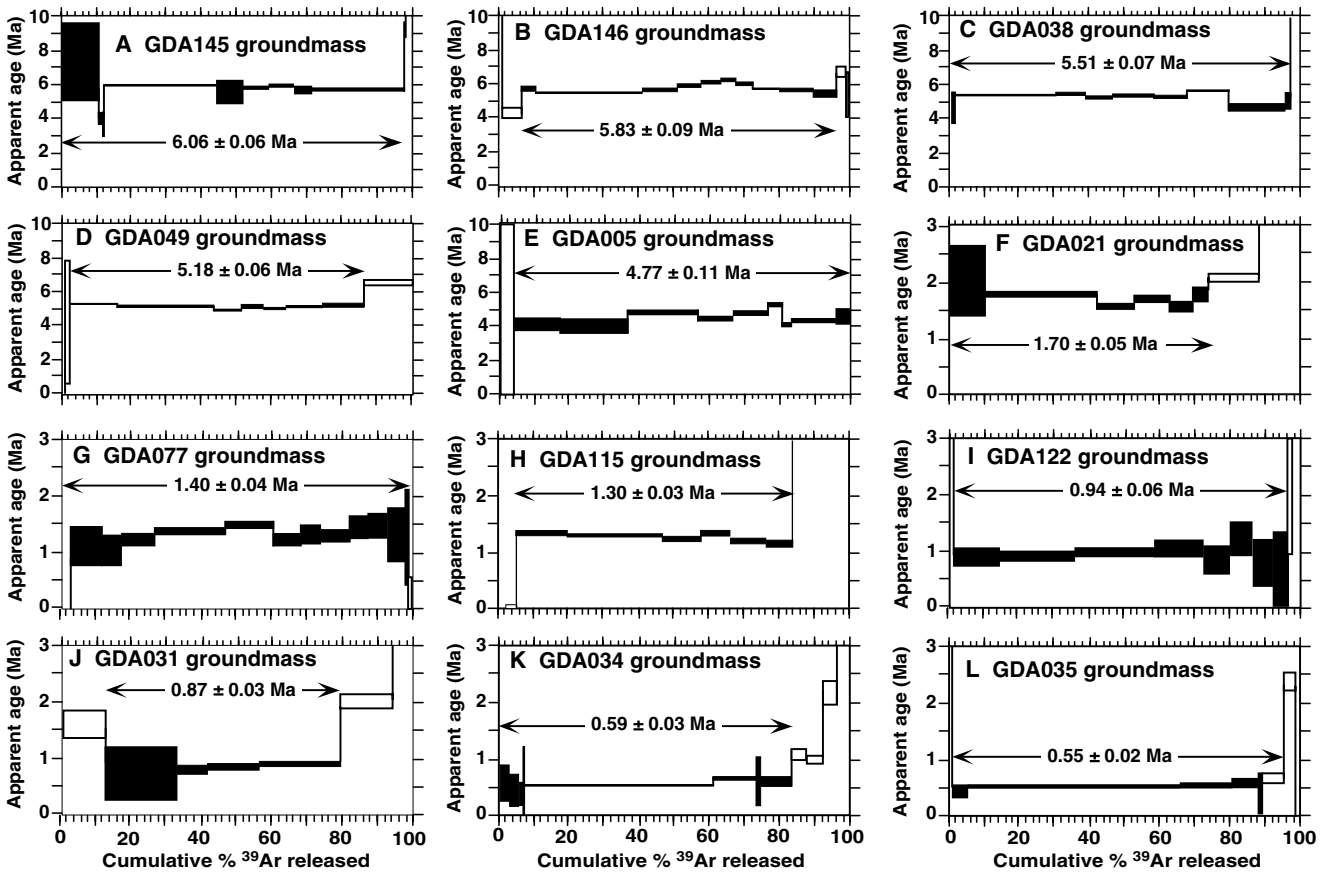

Figure 4. $^{40}Ar/^{39}Ar$ age spectra for C-series basalts from Grenada.

normative; most, but not all, of the most mafic M-series basalts are nepheline normative. Nevertheless, nepheline does not occur as a precipitating phase, and the evolved andesites are all hypersthene or quartz normative. The high apparent normative nepheline content may be partly a consequence of their oxidized nature and hence high Fe^{3+}/Fe^{2+} ratios. Computing norms with higher Fe^{3+}/Fe^{2+} reduces the normative nepheline but generally does not eliminate it. Even assuming a $Fe^{3+}/\Sigma Fe$ as high as 0.54 (Stamper et al., 2014b), many basalts remain nepheline normative.

Arculus (1976) originally named the C and M series as the high-Sr and low-Sr series, respectively. The difference between them is apparent in plots of Sr and CaO versus MgO, as in Figure 8. The more mafic C-series lavas have high Sr and CaO contents, which then rapidly decrease with decreasing MgO. Strontium concentrations in M-series lavas are lower and show little systematic variation with MgO above ~6% MgO, at which point concentrations tend to increase. Calcium oxide also decreases with MgO in M-series basalts, but CaO is typically 40% lower in M-series basalts than in C-series basalts at a given MgO concentration. C-series basalts also have higher FeO* and lower Na_2O (Fig. 9) and slightly lower TiO_2 than the M series at a given MgO concentration, but the two series are indistinguishable on plots of Al_2O_3 and K_2O versus MgO.

Below ~4% MgO, the trends of the two series appear to merge, as is apparent in both Figures 8 and 9. At that point, the series are indistinguishable in every respect, including isotopic composition. We have consequently plotted samples with less than 4% MgO, which corresponds approximately to andesitic compositions (>54% SiO_2) using a separate symbol, including andesitic samples analyzed by Thirlwall et al. (1996), which they assigned to the M series. Even in the range of 4%–6% MgO, the two series can be difficult to distinguish both in hand specimen and on major-element composition. This is a significant observation and one to which we will return later.

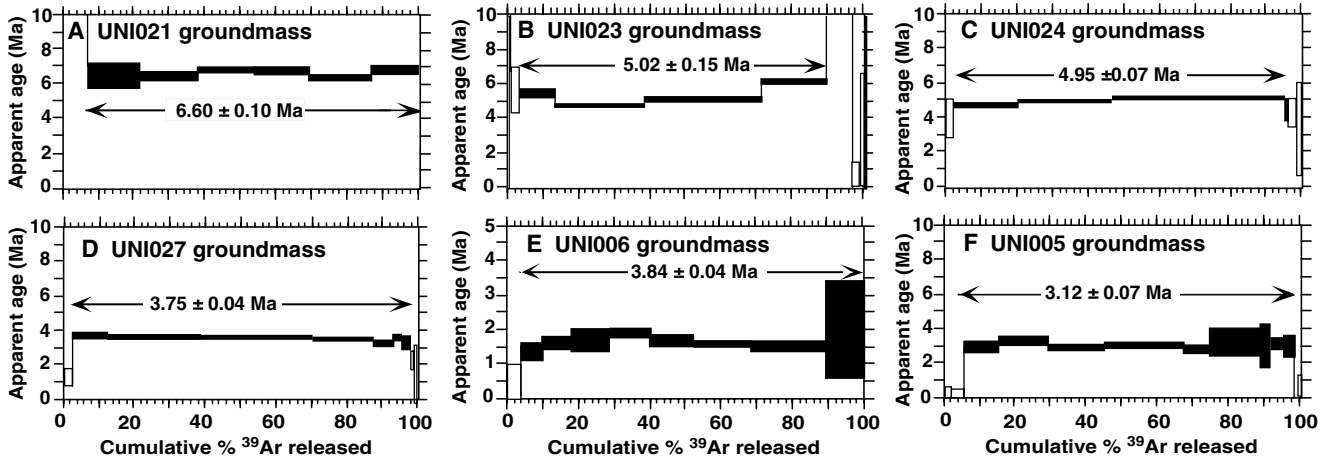

Figure 5. $^{40}Ar/^{39}Ar$ age spectra for basalts from Union Island.

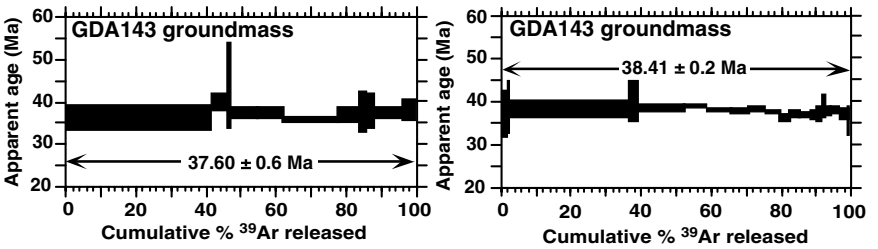

Figure 6. $^{40}Ar/^{39}Ar$ age spectra for dacite dike GDA143 from southernmost Grenada.

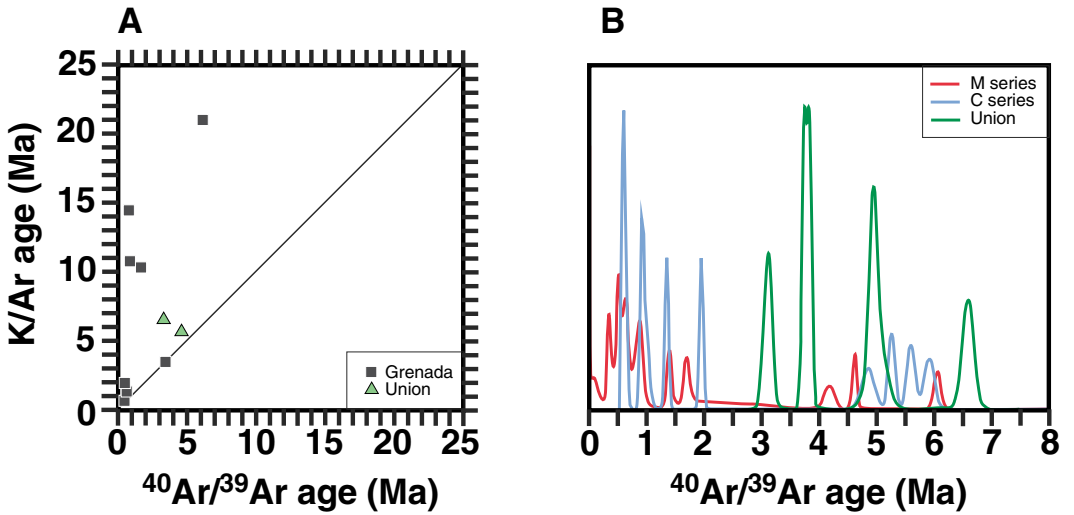

Figure 7. (A) Comparison of K-Ar ages from Briden et al. (1979) with $^{40}Ar/^{39}Ar$ ages for Grenada and Union from this study. K-Ar ages are older, most likely due to inherited ^{40}Ar. (B) Probability density functions of ages of Grenada and Union samples.

TABLE 2. MAJOR-ELEMENT COMPOSITIONS

Sample	GDA005	GDA031	GDA034	GDA035	GDA038GM	GDA049	GDA115	GDA122	GDA146
Series	C	C	C	C	C	C	C	C	C
SiO_2	47.04	50.12	48.64	52.47	47.60	47.61	44.6	45.5	45.55
TiO_2	0.91	1.22	1.13	0.89	1.020	0.99	0.97	0.87	0.83
Al_2O_3	14.74	18.69	17.39	18.11	15.04	16.1	17.63	16.68	15.01
FeO*	9.76	8.99	9.54	7.63	9.78	10.26	11.84	11.72	10.10
MgO	8.9	5.91	5.85	4.76	8.16	7.24	6.51	6.99	7.79
CaO	14.58	11.04	12.77	10.43	14.79	14.05	13.81	14.05	14.54
Na_2O	1.81	2.39	2.49	3.49	1.64	1.93	1.67	1.76	1.84
K_2O	1.07	1.24	1.12	1.41	1.06	1.24	0.95	0.79	1.22
MnO	0.24	0.16	0.16	0.21	0.13	0.17	0.19	0.19	0.16
P_2O_5	0.07	0.28	0.21	0.42	0.31	0.26	0.133	0.15	0.20
Total	99.12	100.04	99.3	99.82	99.53	99.85	98.30	98.7	97.23

Sample	GDA021	GDA030	GDA040	GDA077	GDA084B	GDA124	GDA143	GDA161	GDA162
Series	M	M	M	M	M	M	M	M	M
SiO_2	48.58	48.89	54.03	48.62	43.97	44.43	66.33	47.82	46.86
TiO_2	0.96	0.91	0.73	0.94	0.99	1.51	0.74	0.85	0.86
Al_2O_3	16.41	15.11	18.5	15.14	13.55	12.33	13.93	14.12	13.8
FeO*	9.87	9.55	7.72	9.2	10.00	10.46	6.09	9.13	9.34
MgO	8.01	8.07	3.98	10.26	13.91	13.15	3.02	12.19	14.14
CaO	12.26	12.92	9.12	12.02	12.78	12.86	4.49	11.99	11.45
Na_2O	2.25	2.37	3.34	2.29	2.49	2.96	2.91	2.12	2.2
K_2O	0.57	0.99	0.85	0.72	0.63	0.34	1.71	0.74	0.47
MnO	0.19	0.17	0.17	0.17	0.18	0.19	0.19	0.15	0.19
P_2O_5	0.16	0.25	0.21	0.26	0.37	1.05	0.07	0.30	0.12
Total	99.26	99.23	98.65	99.62	98.87	99.28	99.48	99.41	99.43

Sample	GDA163	GDA043A Hornblende-clinopyroxene	GDA080 Hornblende-clinopyroxene	GDA147 Clinopyroxene	GDA147 Clinopyroxene	GDA143 Eocene	WIC020 Isle de Caille
Series	M	XENO	XENO	XENO	XENO	Dike	M
SiO_2	45.68	46.1	50.05	46.99	47.75	66.33	48.41
TiO_2	1.01	0.05	0.74	0.48	0.52	0.74	0.95
Al_2O_3	14.57	18.59	19.68	14.21	14.8	13.93	16.39
FeO*	9.33	5.82	10.05	9.08	7.48	6.09	8.47
MgO	12.43	12	3.04	7.79	7.54	3.02	10.16
CaO	12.29	13.07	9.59	19.51	19.94	4.49	11.84
Na_2O	2.62	0.7	3.87	0.94	1	2.91	2.22
K_2O	0.97	0.04	1.34	0.01	0.01	1.71	0.46
MnO	0.19	0.1	0.24	0.25	0.25	0.19	0.16
P_2O_5	0.42	0.02	0.33	0.09	0.09	0.07	n.d.
Total	99.51	96.49	98.93	99.35	99.38	99.48	99.06

(*continued*)

TABLE 2. MAJOR-ELEMENT COMPOSITIONS (*continued*)

Sample	MAY002	UNI006	UNI008/005	UNI021	UNI023	UNI024	UNI025	UNI026
Series	Mayreau	Union	Union	Union	Union	Union	Union	Union
SiO_2	52.48	48.11	56.05	50.03	57.83	69.78	52.42	60.50
TiO_2	1.31	0.96	0.66	0.79	0.61	0.36	1.08	0.54
Al_2O_3	16.81	18.54	18.09	16.78	18.42	15.78	18.94	18.27
FeO*	10.21	9.03	7.06	8.42	6.28	2.85	7.89	5.58
MgO	2.75	7.82	3.35	9.47	2.16	0.68	4.70	1.66
CaO	5.4	12.49	8.79	10.75	8.06	4.06	10.40	7.83
Na_2O	4.22	2.20	4.08	2.37	4.34	4.39	2.72	4.33
K_2O	0.49	0.40	1.31	0.83	1.35	1.75	1.46	1.19
MnO	0.09	0.24	0.20	0.19	0.32	0.12	0.19	0.20
P_2O_5	0.11	0.14	n.d.	0.19	0.25	0.09	0.14	0.20
Total	93.87	99.93	99.59	99.82	99.62	99.86	99.94	100.30

Sample	UNI027	UNI028	UNI029	UNI030	UNI032	UNI033	UNI034	UNI035
Series	Union	Union	Union	Union	Union	Union	Union	Union
SiO_2	58.47	49.87	55.66	47.58	51.84	56.39	51.08	56.32
TiO_2	0.57	1.23	1.09	0.91	0.93	0.71	0.93	0.92
Al_2O_3	18.34	20.49	19.25	17.57	18.76	17.32	17.15	20.98
FeO*	5.74	10.06	5.90	9.40	7.73	7.16	7.75	6.61
MgO	1.89	3.84	3.53	8.37	5.24	3.68	6.15	1.67
CaO	8.28	9.90	9.87	13.49	10.52	7.42	12.19	9.12
Na_2O	4.66	2.78	2.69	1.97	2.65	4.86	2.53	3.40
K_2O	1.21	0.59	1.33	0.47	1.29	1.92	0.94	0.92
MnO	0.19	0.30	0.10	0.16	0.14	0.17	0.19	0.27
P_2O_5	0.22	0.20	0.11	0.17	0.17	0.22	0.13	0.38
Total	99.57	99.26	99.53	100.09	99.27	99.85	99.04	100.59

n.d.—not determined.

We have generally used the Sr-MgO and CaO-MgO trends to distinguish between the M and C series. Thus, where Woodland et al. (2002) identify two samples as M-C transitional, we find they plot within the scatter of the M series on Sr-MgO and CaO-MgO, and we have included them in that series, despite some affinities to the C series. Where the major-element compositions of samples in this range are ambiguous as to which series a sample belongs, we have used isotope ratios as additional criteria (see below).

The melt inclusions analyzed by Bouvier et al. (2010) plot mainly within the M-series trends and are distinct from the C series, which is not surprising since the Queen's Park scoria cone, from which these samples were taken, consists of M-series picritic basalt (our sample from this site is GDA008, the major-element composition of which was previously reported by Devine, 1995). However, a few of the inclusions have CaO contents well above those seen in M-series lavas, and in some cases above those of the C series, at comparable MgO. However, their Sr contents never reach those of C-series lavas at comparable MgO contents. The more mafic melt inclusions also tend to be richer in FeO* than M-series lavas.

Our two samples from Isle de Caille fall well within the M-series trend in these figures, and they also have M-series isotopic and trace-element characteristics, and we henceforth treat them as part of the M series. Both Kick 'em Jenny and Union Island fall along the M-series Sr-MgO trend, but the Union basalts tend to have slightly higher CaO concentrations than most M series at comparable MgO concentrations. Both plot slightly to the high Al_2O_3 side of the Al_2O_3-MgO trend defined by the Grenada data. The Na_2O and FeO* concentrations in Union Island lavas exhibit considerable scatter at a given MgO but are perhaps more similar to the Grenada C series than the M series. Kick 'em Jenny lavas follow the M-series FeO*-MgO trend, but Na_2O is intermediate between the M and C series. The K_2O in Kick 'em Jenny samples falls within the broad trend defined by all Grenada samples, while K_2O in Union samples tends to be lower than that in both Grenada series, although they scatter considerably. Our single analyzed sample from Mayreau is a basaltic andesite. Its most distinctive feature compared to the Union and Grenada samples is low K_2O. The low major-element total suggests high water content and indeed the hand specimen appears highly altered.

TABLE 3. ISOTOPE RATIOS AND TRACE ELEMENTS

Sample	GDA005 C series	GDA031 C series	GDA034 C series	GDA038 GM C series	GDA038 CPX C series	GDA038 NMCPX XENO	GDA038 PLAG XENO	GDA035 C series	GDA049 C series	GDA115 C series
$^{87}Sr/^{86}Sr$	0.704530	0.704557	0.704432	0.704395	0.704220			0.704617	0.704294	0.704420
$^{143}Nd/^{144}Nd$	0.513013	0.512902	0.512953	0.512898	0.512925			0.512911	0.512977	0.512960
ε_{Nd}	7.3	5.1	6.1	5.1	5.6			5.3	6.6	6.3
$^{206}Pb/^{204}Pb$	18.863	19.072	18.953	18.930				19.186	19.005	18.803
$^{207}Pb/^{204}Pb$	15.656	15.677	15.684	15.632				15.717	15.644	15.632
$^{208}Pb/^{204}Pb$	38.711	38.675	38.650	38.632				38.859	38.744	38.423
Li	9.18	7.31	11.68			19.78	3.48	15.64	6.71	5.78
Sc	44.4	30.0	38.6			86.6	18.6	24.4	32.7	36.5
V	288.4	307.3	355.2			208.1	291.9	246.8	275.6	377.7
Cr	416.3	65.5	87.7			500.4	91.6	45.5	75.6	35.3
Co	46.6	35.8	41.8			39.7	38.2	31.7	40.5	42.8
Ni	72.6	45.0	71.6			71.7	51.9	49.9	52.8	47.6
Cu	79.6	74.4	91.4			25.4	98.7	269.3	90.2	62.0
Zn	78.6	75.4	108.0			26.0	71.2	61.5	65.4	67.8
Rb	9.5	20.0	19.2	22.9		1.5	19.2	26.9	22.4	11.7
Sr	1880	862	1260	1592		299	2872	1042	1516	1287
Y	20.5	21.8	21.3	21.1		25.9	19.9	20.3	21.6	22.8
Zr	79.7	89.4	85.9	130		85.3	78.8	106.8	92.8	55.3
Nb	3.04	8.70	3.21			0.26	4.37	5.88	3.53	2.46
Cs	0.50	0.27	0.47			0.02	0.17	0.52	0.48	0.69
Ba	303	303	325	478		139	577	420	294	330
La	27.0	14.5	18.2			9.8	33.9	22.5	29.8	11.0
Ce	59.8	33.7	42.7			34.6	67.2	47.0	72.2	26.4
Pr	7.74	4.36	5.20			6.12	7.97	5.25	8.29	3.77
Nd	31.8	19.2	21.6			31.6	30.5	20.9	33.5	17.2
Sm	6.16	4.44	4.71			7.97	5.38	4.35	6.57	4.12
Eu	1.66	1.34	1.41			2.02	1.63	1.27	1.72	1.31
Gd	5.13	3.81	4.01			5.78	4.98	3.79	5.28	4.08
Tb	0.75	0.66	0.65			1.02	0.63	0.57	0.81	0.63
Dy	3.56	3.58	3.48			5.14	3.03	3.09	3.86	3.49
Ho	0.65	0.76	0.69			0.92	0.55	0.62	0.75	0.73
Er	1.53	1.98	1.80			2.16	1.47	1.63	1.93	1.90
Tm	0.25	0.32	0.28			0.32	0.23	0.26	0.29	0.30
Yb	1.40	1.97	1.69			1.80	1.36	1.63	1.72	1.74
Lu	0.20	0.30	0.27			0.27	0.21	0.25	0.28	0.26
Hf	2.25	2.43	2.36			3.14	1.76	2.67	2.38	1.65
Ta	0.08	0.39	0.20			–0.03	0.13	0.36	0.17	0.13
Pb	1.44	2.45	1.76			0.19	1.78	1.89	1.18	1.10
Th	6.07	4.63	6.78			1.05	9.07	10.21	9.87	2.90
U	1.66	2.43	2.76			0.17	2.43	4.65	3.26	1.39

(*continued*)

TABLE 3. ISOTOPE RATIOS AND TRACE ELEMENTS (*continued*)

Sample	GDA122 C series	GDA146 C series	GDA008 M series	GDA011 M series	GDA021 M series	GDA030 M series	GDA040 M series	GDA045 M series	GDA063B M series	GDA077 M series
$^{87}Sr/^{86}Sr$	0.704490	0.704172	0.705125	0.704850	0.705149		0.704962		0.705408	0.705146
$^{143}Nd/^{144}Nd$	0.513020	0.512999	0.512845	0.512880	0.512879		0.512860		0.512790	0.512832
ε_{Nd}	7.5	7.0	4.0	4.7	4.7		4.3		3.0	3.8
$^{206}Pb/^{204}Pb$	18.76	18.852	19.585	19.346	19.307		19.413		19.481	19.328
$^{207}Pb/^{204}Pb$	15.644	15.627	15.853	15.750	15.745		15.740		15.710	15.737
$^{208}Pb/^{204}Pb$	38.470	38.585	39.440	38.967	38.969		38.992		39.035	38.946
Li	5.81	4.94	5.02	5.89	7.42		15.89		9.53	7.44
Sc	39.9	36.9	35.1	36.3	43.6		20.1		34.7	38.6
V	323.6	292.8	198.1	219.0	307.8		170.0		290.3	284.8
Cr	55.7	201.8	958.0	629.1	277.6		73.8		395.3	385.3
Co	43.0	43.6	69.7	56.6	49.8		32.5		56.0	47.3
Ni	51.5	71.1	602.3	415.5	160.5	111	35.4	205	157.0	142.9
Cu	115.2	147.5	36.5	86.8	71.8		39.9		78.8	103.2
Zn	66.8	69.3	70.1	76.4	77.6		70.1		79.0	72.7
Rb	8.7	20.3	8.4	6.6	13.1	27.2	27.0	16	20.1	11.4
Sr	1413	1855	272	305	466	546	501	264	779	542
Y	24.6	20.1	16.4	19.7	19.4	18	20.2	18	21.9	18.6
Zr	68.1	98.1	45.4	70.5	63.1	78	90.4	70	96.7	68.6
Nb	1.95	3.35	3.52	4.69	4.06		10.40		13.55	5.52
Cs	0.27	0.21	0.17	0.23	0.63		1.14		0.95	0.10
Ba	250	248	76	124	242	232	321	136	290	199
La	17.0	28.4	5.6	10.1	9.7		18.4		32.6	14.1
Ce	38.5	57.5	11.0	21.6	21.2		34.8		60.2	30.9
Pr	5.17	8.17	1.76	2.96	2.61		4.19		6.99	3.46
Nd	22.4	32.9	8.0	12.7	11.6		16.2		26.8	14.2
Sm	4.86	6.20	2.08	3.10	3.00		3.53		5.44	3.38
Eu	1.44	1.69	0.70	0.99	1.00		1.13		1.55	1.03
Gd	4.51	5.31	2.31	3.24	3.02		3.45		4.97	3.16
Tb	0.68	0.74	0.42	0.56	0.55		0.58		0.75	0.56
Dy	3.66	3.60	2.53	3.26	3.15		3.38		3.92	3.11
Ho	0.77	0.67	0.54	0.67	0.66		0.71		0.76	0.64
Er	1.95	1.70	1.44	1.82	1.83		1.95		1.93	1.69
Tm	0.30	0.26	0.23	0.28	0.28		0.32		0.31	0.27
Yb	1.80	1.53	1.39	1.70	1.76		2.04		1.84	1.66
Lu	0.27	0.23	0.22	0.28	0.27		0.33		0.28	0.25
Hf	1.88	2.56	1.25	2.03	1.71		2.58		2.50	1.75
Ta	0.12	0.18	0.19	0.24	0.24		4.37		5.89	0.33
Pb	1.25	2.38	1.07	2.09	2.25		3.22		4.38	2.24
Th	4.56	7.81	1.57	2.29	2.97		5.89		11.36	5.18
U	1.57	2.24	0.49	0.40	1.05		3.42		4.00	2.13

(*continued*)

TABLE 3. ISOTOPE RATIOS AND TRACE ELEMENTS (*continued*)

Sample	GDA084B M series	GDA124 M series	GDA138 M series	GDA145 M series	GDA161 M series	GDA162 M series	GDA163 M series	X28118 M series	X28147 M series	X28173 M series
$^{87}Sr/^{86}Sr$	0.705599	0.706170	0.704933	0.705125					0.705147	0.705429
$^{143}Nd/^{144}Nd$	0.512728	0.512570	0.512847	0.512782					0.512851	0.512693
ε_{Nd}	1.8	–1.3	4.1	2.8					4.1	1.1
$^{206}Pb/^{204}Pb$	19.392	19.281	19.437	19.601					19.259	19.340
$^{207}Pb/^{204}Pb$	15.737	15.704	15.756	15.733					15.724	15.724
$^{208}Pb/^{204}Pb$	39.118	39.064	39.059	39.164					38.883	39.060
Li	8.65	10.32	5.78	6.00					6.11	6.29
Sc	35.1	32.9	35.2	8.7					41.2	41.0
V	247.7	265.0	238.5	166.0					302.3	274.8
Cr	675.9	629.4	1147.2	6.6					629.1	727.2
Co	50.1	51.2	55.4	16.4					50.1	56.0
Ni	291.6	290.0	372.6	13.5	245	350	280	226	207.2	289.1
Cu	103.2	91.6	67.4	19.8					76.8	79.6
Zn	70.1	79.1	68.2	66.8					59.2	76.2
Rb	18.0	59.6	10.3	49.0	18	12	28	21	9.9	23.3
Sr	799	970	343	1241	625	342	841	308	410	559
Y	19.7	22.6	17.2	22.6	23	24.	22.0	20	18.4	18.9
Zr	121.9	338.2	56.9	25.8	97	67	166.	80	53.9	128.6
Nb	9.65	33.30	3.95	14.51					3.76	10.96
Cs	1.07	4.55	0.45	1.15					0.27	0.93
Ba	354	889	100	231				258	122	402
La	31.4	58.3	6.2	27.2					9.8	22.0
Ce	66.7	115.6	12.5	53.0					20.3	47.2
Pr	7.41	14.41	2.03	6.94					2.72	5.49
Nd	28.2	54.1	9.3	26.6					11.8	21.7
Sm	5.29	9.43	2.45	5.12					3.09	4.40
Eu	1.45	2.37	0.81	1.41					0.97	1.26
Gd	4.83	7.74	2.64	4.41					3.13	4.15
Tb	0.69	1.01	0.47	0.68					0.56	0.63
Dy	3.51	4.56	2.77	3.63					3.22	3.37
Ho	0.68	0.80	0.58	0.72					0.68	0.67
Er	1.71	1.91	1.54	1.89					1.79	1.75
Tm	0.27	0.28	0.25	0.31					0.30	0.27
Yb	1.58	1.58	1.46	1.91					1.73	1.59
Lu	0.23	0.23	0.23	0.29					0.28	0.25
Hf	3.86	8.63	1.55	0.92					1.70	3.35
Ta	0.45	1.82	0.24	0.82					0.24	0.55
Pb	7.86	11.05	2.10	4.79					1.98	4.21
Th	14.50	28.01	1.64	15.27					2.80	11.30
U	4.99	7.83	0.65	5.59					0.92	3.48

(*continued*)

TABLE 3. ISOTOPE RATIOS AND TRACE ELEMENTS (*continued*)

Sample	X28182 M series	X28326 M series	X28348 M series	X28367 M series	WIC018 Isle de Caille M series	WIC020 Isle de Caille M series	KEJ017A Kick 'em Jenny	KEJ101 Kick 'em Jenny	K1 Kick 'em Jenny	GDA037 THF sediment
$^{87}Sr/^{86}Sr$	0.705082	0.705135	0.704786	0.705672	0.705150	0.705190	0.705571	0.705841	0.705730	0.705116
$^{143}Nd/^{144}Nd$	0.512895	0.512884	0.512922	0.512620	0.512820	0.512822	0.512893	0.512867	0.512828	0.512627
ε_{Nd}	5.0	4.8	5.5	-0.3	3.6	3.6	5.0	4.5	3.7	-0.2
$^{206}Pb/^{204}Pb$	19.540	19.389	19.433	19.427	19.534	19.408	19.545	19.721	19.645	19.395
$^{207}Pb/^{204}Pb$	15.784	15.780	15.771	15.748	15.760	15.750	15.763	15.786	15.751	15.702
$^{208}Pb/^{204}Pb$	39.164	39.094	39.094	39.154	39.147	39.307	39.152	39.262	39.132	38.942
Li	6.92	6.51	6.81	7.92	6.79		6.62	7.84		41.90
Sc	49.0	44.3	38.6	34.3	43.0		46.2	50.5	32.6	23.4
V	312.5	285.9	241.8	265.6	257.8		276.9	322.7		191.7
Cr	502.5	789.6	742.4	499.9	507.0		400.1	138.2	319.0	22.6
Co	49.8	56.2	50.0	49.5	48.8		42.7	33.3	26.2	6.3
Ni	182.6	301.5	317.2	247.5	225.8		173.7	69.9	1211.0	36.6
Cu	112.1	89.0	53.8	73.4	82.0		91.3	82.9		73.3
Zn	72.0	73.6	68.9	80.2	66.8		71.0	70.5	81.0	94.6
Rb	10.1	10.7	6.9	19.8	11.6	8.5	16.1	21.2	340.0	18.7
Sr	332	402	355	625	272	285	303	306	24	636
Y	18.6	18.6	19.7	20.5	19.3		20.3	22.2	96.0	43.0
Zr	57.5	64.5	91.4	138.4	60.4		57.0	69.6		89.1
Nb	3.34	4.03	4.74	12.20	3.80		3.72	4.62		2.00
Cs	0.32	0.51	0.07	3.47	1.04		0.53	0.62	1.20	1.19
Ba	104	131	111	350	130		94	128	178	204
La	8.4	8.5	8.4	30.2	5.5		3.9	5.4	8.8	21.4
Ce	18.6	20.0	18.5	63.2	13.0		9.9	13.2	19.4	11.3
Pr	2.39	2.67	2.44	7.68	1.79		1.44	1.81		5.51
Nd	10.7	12.0	10.6	29.5	8.0	8	6.9	8.3	11.1	24.6
Sm	2.84	3.14	2.72	5.59	2.22	2.29	2.11	2.51	2.79	6.05
Eu	0.91	0.97	0.89	1.57	0.76		0.73	0.86	0.99	1.59
Gd	3.17	3.25	3.01	5.07	2.52		2.53	3.03		5.20
Tb	0.54	0.53	0.52	0.76	0.48		0.48	0.56	0.59	1.08
Dy	3.24	3.03	3.08	3.88	2.94		3.02	3.57		6.37
Ho	0.68	0.62	0.65	0.76	0.64		0.66	0.78		1.39
Er	1.80	1.62	1.79	1.93	1.79		1.81	2.19		3.58
Tm	0.29	0.25	0.29	0.31	0.29		0.30	0.36		0.60
Yb	1.71	1.48	1.77	1.81	1.74		1.78	2.15	2.35	3.50
Lu	0.27	0.23	0.28	0.28	0.27		0.27	0.34	0.37	0.54
Hf	1.56	1.63	2.09	3.97	1.95		1.48	1.89	2.57	2.53
Ta	0.19	0.22	0.25	0.74	0.20		0.17	0.24	0.36	0.05
Pb	2.59	2.95	1.63	6.51	1.82	1.76	3.60	4.21		4.24
Th	3.05	2.76	3.17	13.15	1.74	1.76	1.42	2.34	2.97	1.30
U	0.97	1.20	1.14	4.09	0.71	0.69	0.70	1.18	1.52	0.81

(*continued*)

TABLE 3. ISOTOPE RATIOS AND TRACE ELEMENTS (*continued*)

Sample	GDA086 THF sediment	GDA131 AMPH	GDA033 GM XENO	GDA033 AMPH XENO	GDA080 HF XENO	GDA043A XENO	GDA043B XENO	GDA080 XENO	GDA081 Interstitial glass	GDA091 CPX XENO
$^{87}Sr/^{86}Sr$	0.705091	0.704939	0.705191			0.704299	0.703781	0.705070	0.705086	0.705063
$^{143}Nd/^{144}Nd$		0.512924	0.512822			0.512951	0.512968	0.512838		
ε_{Nd}		5.58	3.59			6.1	6.4	3.9		
$^{206}Pb/^{204}Pb$	19.982	19.421	19.303			19.525	19.462		19.231	19.284
$^{207}Pb/^{204}Pb$	15.747	15.736	15.703			15.707	15.768		15.563	15.708
$^{208}Pb/^{204}Pb$	38.876	38.998	38.842			38.982	39.141		38.666	38.839
Li				4.30	2.33		10.66	3.14		
Sc				48.8	95.7		19.0	68.9		
V				387.4	232.7		66.9	390.8		
Cr				527.5	1065.4		455.2	332.1		
Co				53.2	39.3		41.3	52.6		
Ni				243.5	132.2		326.4	176.4		
Cu				13.6	9.5		10.5	28.8		
Zn				52.0	30.5		25.5	46.7		
Rb				2.9	0.7		0.9	4.0		
Sr				364	94		171	397		
Y				24.7	14.7		5.8	19.0		
Zr				38.7	39.0		1.6	48.7		
Nb				5.15	0.45		0.32	3.77		
Cs				0.01	0.03		0.02	0.39		
Ba				98.2	16.6		62.0	119.4		
La				2.5	1.6		1.6	4.8		
Ce				12.3	8.0		1.1	14.7		
Pr				2.38	1.54		0.42	2.59		
Nd				13.1	8.6		1.9	13.4		
Sm				4.20	2.70		0.51	4.04		
Eu				1.25	0.75		0.30	1.19		
Gd				3.17	2.06		0.68	3.84		
Tb				0.73	0.45		0.12	0.66		
Dy				4.27	2.66		0.76	3.63		
Ho				0.86	0.53		0.17	0.71		
Er				2.17	1.31		0.46	1.78		
Tm				0.34	0.20		0.08	0.26		
Yb				1.88	1.16		0.42	1.46		
Lu				0.27	0.16		0.07	0.22		
Hf				1.54	1.58		0.05	1.95		
Ta				0.24	–0.02		0.01	0.23		
Pb				0.43	0.15		0.59	0.86		
Th				0.07	0.09		0.08	0.63		
U				0.01	0.05		0.07	0.23		

(*continued*)

TABLE 3. ISOTOPE RATIOS AND TRACE ELEMENTS (*continued*)

Sample	GDA147CNV XENO	GDA147CWV XENO	Mayreau MAY002	Mayreau MAY002 CPX	Union UNI006	BHVO-1 standard	Error (%)(±1σ)
$^{87}Sr/^{86}Sr$	0.704790	0.704801	0.704295		0.705026		
$^{143}Nd/^{144}Nd$	0.512884	0.512833	0.513106	0.513133	0.512800		
ε_{Nd}	4.8	3.8	9.1	9.6	3.2		
$^{206}Pb/^{204}Pb$	19.253	19.215	19.133		19.413		
$^{207}Pb/^{204}Pb$	15.727	15.712	15.660		15.717		
$^{208}Pb/^{204}Pb$	38.915	38.844	38.676		38.862		
Li	2.45	2.74	10.56		5.11		
Sc	36.0	31.7	34.4		32.8	30.42	1.0
V	191.5	127.6	240.9		291.3	314.20	0.8
Cr	383.5	271.1	45.9		155.1	288.05	1.6
Co	45.9	41.4	28.0		45.4	45.11	2.8
Ni	112.2	103.8	30.0		84.5	119.68	1.3
Cu	34.3	12.2	8.1		82.7	136.77	0.9
Zn	50.0	40.1	68.2		75.7	109.41	1.1
Rb	0.3	0.4	7.8		7.7	9.12	1.0
Sr	316	279	226		436	401.18	1.5
Y	15.2	16.5	28.6		18.4	29.15	0.8
Zr	45.4	44.4	78.3		71.6	179.16	1.9
Nb	0.36	1.62	0.71		3.71	19.10	2.8
Cs	0.01	0.00	4.96		0.12		
Ba	17.6	17.3	75.6		102	134.53	2.1
La	3.0	4.5	3.3		9.3	16.22	2.8
Ce	6.4	11.6	10.5		22.1	40.40	2.1
Pr	1.13	2.06	1.76		2.81	5.69	3.9
Nd	5.3	9.4	9.0		12.2	25.05	3.4
Sm	1.56	2.20	3.02		2.95	6.30	2.4
Eu	0.46	0.55	1.00		0.89	2.00	2.4
Gd	1.80	2.20	3.28		2.53	6.18	1.6
Tb	0.36	0.41	0.76		0.51	1.02	1.8
Dy	2.31	2.49	4.54		3.01	5.39	1.9
Ho	0.50	0.54	0.99		0.65	1.02	1.4
Er	1.35	1.49	2.71		1.75	2.48	1.6
Tm	0.22	0.24	0.44		0.29	0.35	2.4
Yb	1.35	1.52	2.62		1.73	2.04	2.1
Lu	0.22	0.23	0.40		0.26	0.30	2.8
Hf	1.29	1.13	2.11		1.73	4.53	2.3
Ta	0.05	0.14	0.06		0.14	1.17	4.2
Pb	0.58	0.45	2.17		1.17	2.05	1.1
Th	0.22	0.96	0.06		1.49	0.48	4.3
U	0.12	0.29	0.36		0.62	1.54	4.6

Abbreviations: AMPH—amphibole; CPX—clinopyroxene; NMCPX—normal clinopyroxene; THF—Tufton Hall Formation; XENO—xenocryst.

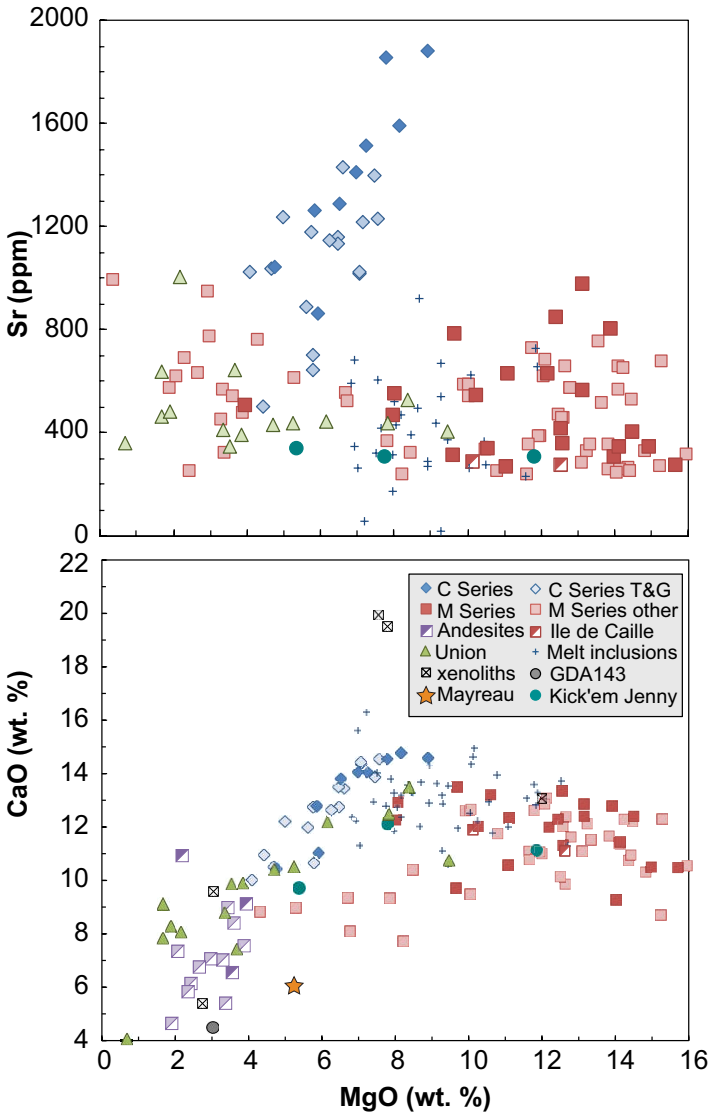

Figure 8. Calcium oxide and Sr as functions of MgO content in samples analyzed in this and earlier studies. On this and subsequent plots, data reported by Devine (1995) and White and Dupré (1986) are plotted with the same symbols as data reported in Tables 1–3. C-series data from Thirlwall and Graham (1984) are labeled as "C-series T&G"; M-series data from Thirlwall and Graham (1984) and other studies, mainly but not exclusively, and Thirlwall et al. (1996) are labeled as "M series other." These data are plotted with symbols with fainter color. Andesitic lavas of both series are effectively indistinguishable and are shown as half-filled purple squares (the darker shades are our analyses; light shades are published analyses). Also shown are melt-inclusion compositions from M-series lava reported by Bouvier et al. (2010).

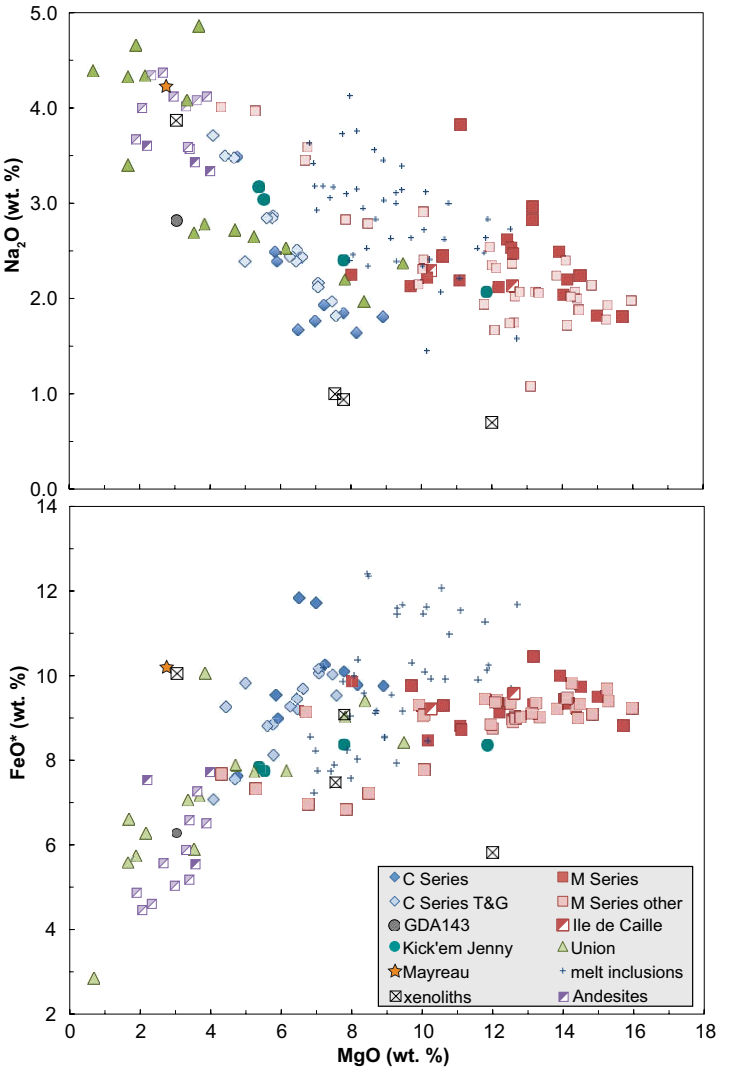

Figure 9. FeO* (total Fe reported as FeO) and Na_2O as a function of MgO in samples analyzed in this and earlier studies. Also shown are melt-inclusion compositions from Bouvier et al. (2010). Symbols are the same as in Figure 8.

Figure 10 compares REE patterns of samples analyzed in this study. As Thirlwall et al. (1996) previously pointed out, the M series exhibits a range in light rare-earth element (LREE) enrichment, with La/Sm_{EF}, i.e., chondrite-normalized La/Sm ratios, ranging from 1.5 to 5.4. The range of La/Sm_{EF} in the C series is smaller, 1.65–3.2, and the range in absolute concentrations is notably lower (for clarity, individual C-series patterns are not shown). This remains true when only the more mafic members of both series are considered. Kick 'em Jenny lavas are less LREE enriched, and their heavy rare-earth element (HREE) contents tend to be higher than most Grenadian lavas of either series. The single Union Island sample we analyzed plots well within the range of the M series. The pattern exhibited by the Mayreau sample is distinct in being LREE depleted. While LREE-depleted patterns do occur among island-arc volcanic rocks, including some from the northern Lesser Antilles, they are more common among lavas erupted at divergent margins, such as mid-ocean ridges. The Tufton Hall Formation sample (GDA037) is modestly LREE enriched, La/Sm_{EF} = 2.18, with relatively high concentrations of heavy rare earths and a large negative Ce anomaly, suggesting a significant seawater-derived component.

Figure 11 illustrates the incompatible trace-element patterns of these samples as well as the xenoliths we analyzed. For clarity, only the ranges observed in the Grenadian lavas and xenoliths are shown, with the Kick 'em Jenny samples included with the M series. Again, the range of compositions in the C series is relatively narrow compared to that of the M series, and the Union sample plots within the range of the M series. The C-series basalts differ from the M series in their strong Sr enrichment as well as in their modest relative depletion in Pb. Xenoliths have generally lower incompatible-element concentrations and exhibit a wide variety of patterns, consistent with an origin as cumulates of variable mineralogy. All samples exhibit some degree of Ta-Nb depletion, as is typical of island-arc volcanics. In this respect, the Mayreau sample differs from mid-ocean ridge basalts but not necessarily from backarc basin basalts.

The Sr- and Nd-isotope ratios are shown in Figure 12. All data shown in this and subsequent figures are measured ratios (not age corrected). Our new data largely overlap data reported in early studies, although they extend the range of the M series somewhat to more radiogenic Sr and less radiogenic Nd. C-series ε_{Nd} values overlap the less radiogenic values observed in mid-ocean ridge basalt (MORB), but, as is typical of IAV, are offset to higher $^{87}Sr/^{86}Sr$ values, and that offset is somewhat greater than in lavas from St. Vincent, the next major volcanic island to the north. The M series ranges to much more "enriched" Sr and Nd isotopic signatures. Notably, all Grenadian andesites and dacites have M-series–like isotopic compositions. Kick 'em Jenny is somewhat offset from the M-series field to higher $^{87}Sr/^{86}Sr$ ratios. The two Isle de Caille samples have very similar Sr and Nd isotopic compositions and plot well within the M-series field, as does the single analyzed sample from Union Island. The ε_{Nd} of the Mayreau sample is +9.6, close to the average value for Atlantic MORB, but the sample has higher $^{87}Sr/^{86}Sr$ than is typical of MORB; however, this may be the result of secondary alteration. Xenolith isotopic compositions largely overlap those of the lavas, although compositions do not range to the extreme values seen in some M-series lavas.

There is some isotopic disequilibrium between separated groundmass and clinopyroxene in C-series basalt GDA038: $^{87}Sr/^{86}Sr$ is lower and ε_{Nd} is higher in the clinopyroxene than in the groundmass, although both ratios in both phases fall within the range of other C-series basalts. On Figure 12, the clinopyroxene is shown with a "C" inside the symbol, and a tie-line

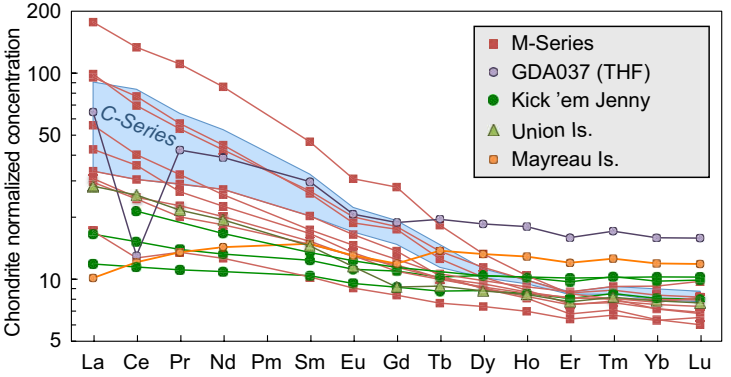

Figure 10. Ordinary chondrite-normalized, rare-earth element patterns in analyzed samples. Rare-earth element (REE) patterns of the C series are less variable than those of the M series. Rare-earth element patterns of Kick 'em Jenny are less light rare-earth–enriched than those of Grenada. The Mayreau sample has a light rare-earth–depleted pattern similar to that of mid-ocean ridge or backarc basin basalts.

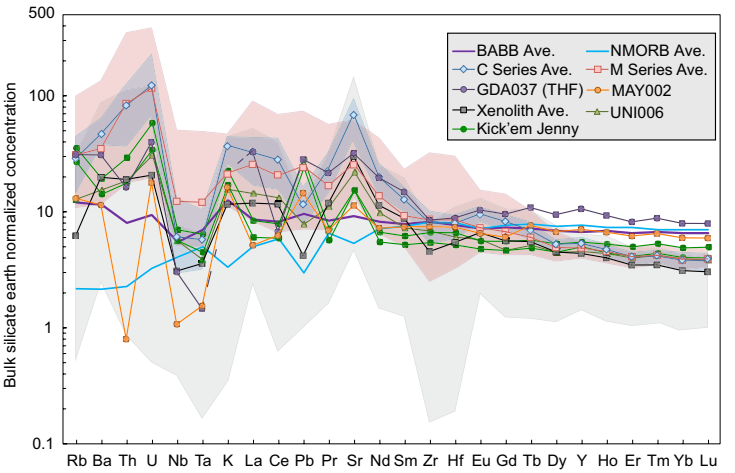

Figure 11. Bulk silicate-earth–normalized concentrations of incompatible elements in samples analyzed in this study. Blue, red, and gray fields show the range of patterns for the C series, M series, and xenoliths, respectively. Bulk silicate-earth composition from McDonough and Sun (1995). Abbreviations: BABB—backarc basin basalt; NMORB—normal mid-ocean ridge basalt.

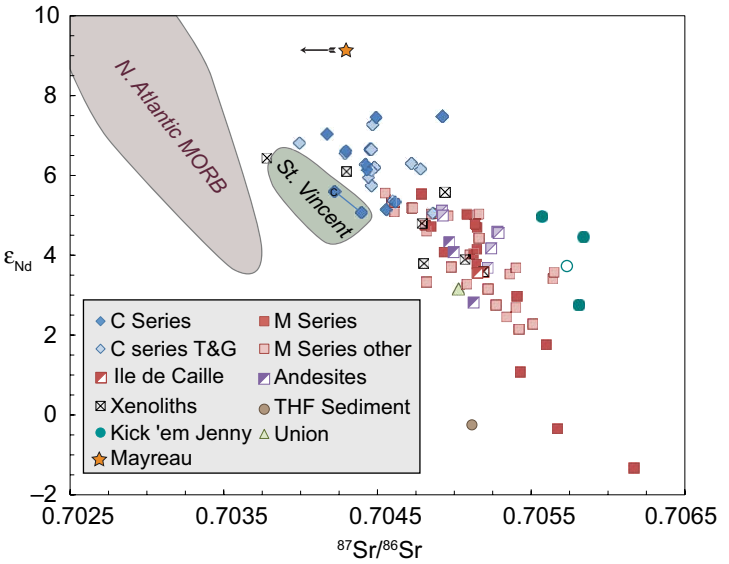

Figure 12. Strontium- and Nd-isotope ratios in samples analyzed in this and earlier studies (Thirlwall and Graham, 1984; Thirlwall et al., 1996, Turner et al., 1996). Separated clinopyroxene from C-series sample GDA038 is shown with a "C" inside the symbol and connected with a tie-line to the separated groundmass. Otherwise, data sources and symbols are the same as in Figure 8.

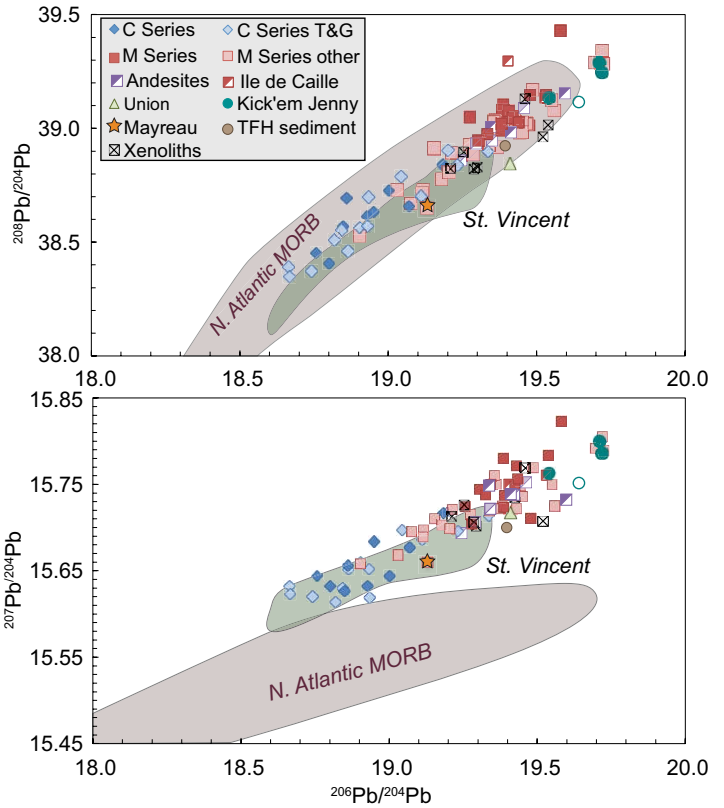

Figure 13. Lead-isotope ratios analyzed in this and earlier studies. Data sources and symbols are the same as in Figure 8. Data reported by Thirlwall and Graham (1984) and Thirlwall et al. (1996) are present-day values rather than the age-corrected values they reported.

connects the clinopyroxene and groundmass. This disequilibrium suggests assimilation or magma mixing during magma evolution, as we discuss in a subsequent section.

Pb-isotope ratios are shown in Figure 13. As discussed in the previous section, the 20 Ma age for the Northern Domes assumed by Thirlwall et al. (1996) is in error. We have calculated measured, present-day Pb-isotope ratios for their samples and used these in Figure 13 in place of the 20 Ma initial ratios they reported. Our new data fall mostly within the range of previously reported data, with the M series having more radiogenic Pb than the C series. Again, the Union sample falls within the M-series range (although they have a bit lower $^{208}Pb/^{204}Pb$). Kick 'em Jenny falls at the extreme end of the M-series range. Most xenoliths also fall within the M-series range. Although they overlap the MORB range in $^{206}Pb/^{204}Pb$ and $^{208}Pb/^{204}Pb$, Grenadian lavas plot to higher $^{207}Pb/^{204}Pb$ ratios than MORB, which has been recognized since Armstrong (1971) as a result of subducted sediment in island-arc magmas and the Lesser Antilles in particular. Indeed, both Grenada and St. Vincent Pb isotopic compositions are shifted toward the field of Pb isotopic compositions of sediments on the adjacent Atlantic plate (Carpentier et al., 2008; White et al., 1985). The Mayreau sample has elevated $^{207}Pb/^{204}Pb$ relative to MORB, indicating an island-arc affinity. Thirlwall et al. (1996) pointed out that both trace-element and isotopic compositions of the M series require a distinctly heterogeneous source, and this is particularly apparent in the relation between ε_{Nd} and $^{206}Pb/^{204}Pb$ shown in Figure 14. Thirlwall et al. (1996) divided the M series into two groups based on ε_{Nd} and La/Y. Several of our new analyses extend toward their low ε_{Nd} group and suggest a continuum of compositions rather than distinct groups.

The Pb isotopic composition of our Tufton Hall Formation is quite similar to the analyses reported by Thirlwall et al. (1996), and all samples have $^{206}Pb/^{204}Pb$ and $^{208}Pb/^{204}Pb$ falling within the range of the M series but with somewhat less radiogenic $^{207}Pb/^{204}Pb$. The Nd isotopic composition of our Tufton Hall sample is significantly less radiogenic than values reported by Thirlwall et al. (1996), suggesting considerable heterogeneity in Tufton Hall isotopic composition.

Xenoliths are occasionally found in Grenada lavas. With the exception of rare peridotites, these are cumulates or metamorphosed cumulates (Arculus

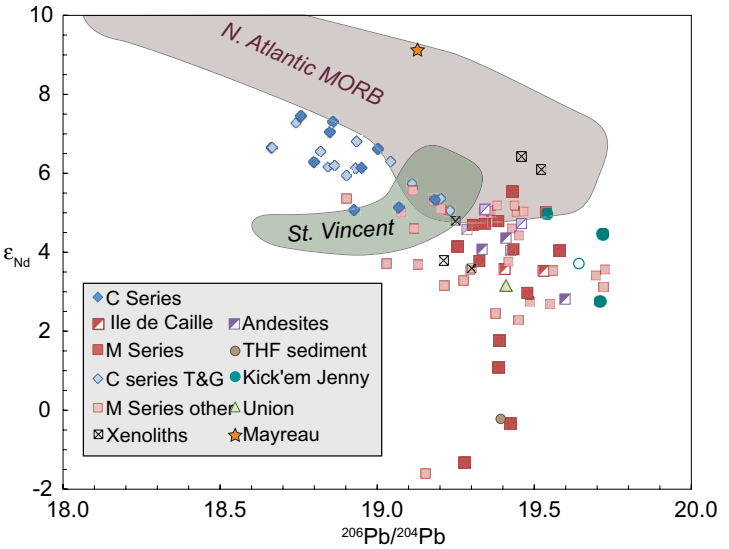

Figure 14. Lead- and Nd-isotope ratios analyzed in this and earlier studies. Data sources and symbols are the same as in Figure 8.

and Wills, 1980). The xenoliths included in this study consist primarily of calcic augite and hornblende with lesser amounts of plagioclase, olivine, and magnetite. Several are notably CaO rich (Fig. 8), reflecting the abundance of augite. Isotopic compositions of these xenoliths range from C series–like to M series–like. Some have textures that are more metamorphic than igneous, suggesting complex histories of recrystallization within the arc crust. Perhaps not surprisingly then, it is difficult to relate their compositions to the magmatic evolution of the lavas.

DISCUSSION

Geochronology and Geochemistry of the Grenadines

Previously reported K-Ar ages of Union Island lavas range from 3.9 to 7.0 Ma (Briden et al., 1979; Westercamp, 1988). Three of our six $^{40}Ar/^{39}Ar$ ages are younger than this (although not dramatically so), indicating volcanic activity on Union Island ceased later than previously thought. Speed et al. (1993) mapped the eastern end of the island as older than the remainder. Our single sample from this area, UNI021, is indeed older at 6.6 Ma than samples farther west, but we obtained ages as old as 5 Ma in the area they map as "younger rocks"; so the distinction does not appear to be dramatic.

According to Speed and Walker (1991), the basement of the Grenadine Platform consists of oceanic crust that was originally part of the Grenada Basin and was uplifted in the late Neogene during the development of the present island arc. They interpret pillow basalts interspersed with Eocene limestones outcropping on Mayreau as part of this oceanic crust. Our single Mayreau sample is LREE depleted (Fig. 10) and has MORB-like Nd-isotope ratios (Fig. 12). Although the $^{87}Sr/^{86}Sr$ is well above MORB values, the Mayreau basalts are extensively altered with loss-on-ignition values ranging from 7% to 16% (Speed and Walker, 1991). The high $^{87}Sr/^{86}Sr$ likely reflects this alteration rather than the original magmatic value. The extended rare-earth pattern (Fig. 11) of the Mayreau basalt, however, reveals several features that differ from those of MORB. Although the uranium and alkali enrichment are almost certainly at least partly a consequence of alteration, the depletion in Nb and Ta and enrichment in Pb cannot be so explained. In addition, its $^{207}Pb/^{204}Pb$ ratio plots above the MORB field on the $^{207}Pb/^{204}Pb$–$^{206}Pb/^{204}Pb$ diagram (Fig. 13). These features are characteristic of subduction-related magmas. This combination of MORB-like and island-arc–like geochemistry is characteristic of backarc basin basalts. The composition of this sample would thus support the interpretation that the Grenada Basin developed through backarc spreading, and the Grenadine Platform consists of crust created in this way and subsequently uplifted (e.g., Speed and Walker, 1991).

The chemistry of Union Island volcanic rocks is intermediate between that of the C and M series of Grenada. Calcium oxide and FeO* concentrations in Union Island basalts are intermediate between those of the two Grenada series, although Na_2O for a given MgO is similar to or lower than the C series. On the other hand, Union Island Sr concentrations are more similar to the M series as is the REE pattern (Fig. 10) and isotopic composition (Figs. 12–14) of the single sample for which we have data. Thus, rather than two distinct magma series, only one of intermediate character is present on Union Island. In addition, differentiated rocks predominate on Union, whereas basalts predominate on Grenada. Partial chemical analyses of additional Union Island samples reported by Thirlwall et al. (1994) support the later observation. Differentiated rocks appear to predominate on several other Grenadine islands, including Cannouan, Mystique, and Bequia, but basalts predominate on Carrioacou, judging from data reported by Thirlwall et al. (1994). There are too few complete analyses from those islands to comment further on how their compositions compare to those of Union and Grenadian lavas.

Kick 'em Jenny

In contrast to Isle de Caille and neighboring Ronde Island, both of which are small volcanic structures that rise only 100 m above the Grenadine Platform, Kick 'em Jenny is located on the eastern slope of the Grenada Basin, rising from depths of greater than 600 m to 178 m (Watlington et al., 2002) and has erupted lavas ranging from magnesian basalt to andesite over the past century. The basalts are unusual in that they contain megacrysts of paragasitic amphibole (Sigurdsson and Shepherd, 1974). Devine and Sigurdsson (1995) found that magnesian Kick 'em Jenny basalts are richer in Al_2O_3 and poorer in CaO than Grenadian M-series basalts at a given MgO. In addition, both melt-

inclusion and whole-rock compositions define a liquid line of descent distinct from that of the M series. These observations suggest Kick 'em Jenny is a distinct volcano unrelated to Grenada. Our data are consistent with this: Kick 'em Jenny lavas have higher $^{87}Sr/^{86}Sr$ for a given ε_{Nd} than the field defined by the M series (Fig. 12), and they have higher Pb-isotope ratios than most M-series lavas (Figs. 13 and 14). They also tend to have flatter rare-earth patterns than M-series lavas (Fig. 10).

Devine and Sigurdsson (1995) suggested that amphibole phenocrysts observed in Kick 'em Jenny basalts were xenocrystic, and assimilation of them influenced compositional evolution in an AFC process. This is consistent with the general observation that amphibole is not stable in basaltic liquids except at very high water contents and high, lower-crustal pressures (e.g., Grove et al., 2003; Pichavant and Macdonald, 2007). Huang et al. (2011) suggested a somewhat similar model involving assimilation of a partial melt of hornblende-bearing andesite in the arc crust to explain U-decay series isotopic variations in Kick 'em Jenny lavas. This "auto-assimilation," that is, assimilation of previously emplaced related igneous rocks within the volcanic edifice, is consistent with the lack or correlation between $^{87}Sr/^{86}Sr$ and indices of differentiation noted by Huang et al. (2011). Such auto-assimilation would not explain the isotopic differences between Grenada and Kick 'em Jenny, however, and we conclude that Kick 'em Jenny is a distinct volcano and not directly related to Grenada.

Geochronology of Grenada

No systematic, statistically significant temporal variations in composition are observed over time, but the data hint at some possible ones (Fig. 15). The younger C-series lavas appear to be more differentiated than the older ones (the older ones have MgO >7%, the younger ones <7%), and the lowest ε_{Nd} and highest $^{87}Sr/^{86}Sr$ ratios (not shown) occur only among the younger M-series lavas. On the other hand, $^{206}Pb/^{204}Pb$ shows no variation with time, nor do incompatible element ratios such as La/Sm (not shown). The main observations to be drawn are that compositions of lavas erupted on Grenada have changed little over the past 6 million years, and eruption of C- and M-series lavas has been interspersed in both time and space. Indeed, both C- and M-series basalts have apparently been erupted from all five major volcanic centers in Grenada identified by Arculus (1976) over the past 6 million years. Our two analyzed samples from Isle de Caille fall well within the range of the Grenada M-series compositions. Thus, although strictly part of the Grenadines, these basalts appear to be part of the Grenadian volcanic system. Given that the ages of these flows are likely less than 1000 years (Turner et al., 2001), they represent the youngest episode of Grenadian volcanism. We have only major-element data for the Eocene dacitic dike crosscutting the Tufton Hall Formation on Grenada. Although dacitic compositions have been observed among backarc basin magmas, they are relatively uncommon. Furthermore, the major-element composition of this sample plots within the compositional trends defined by Neogene magmatism on Grenada.

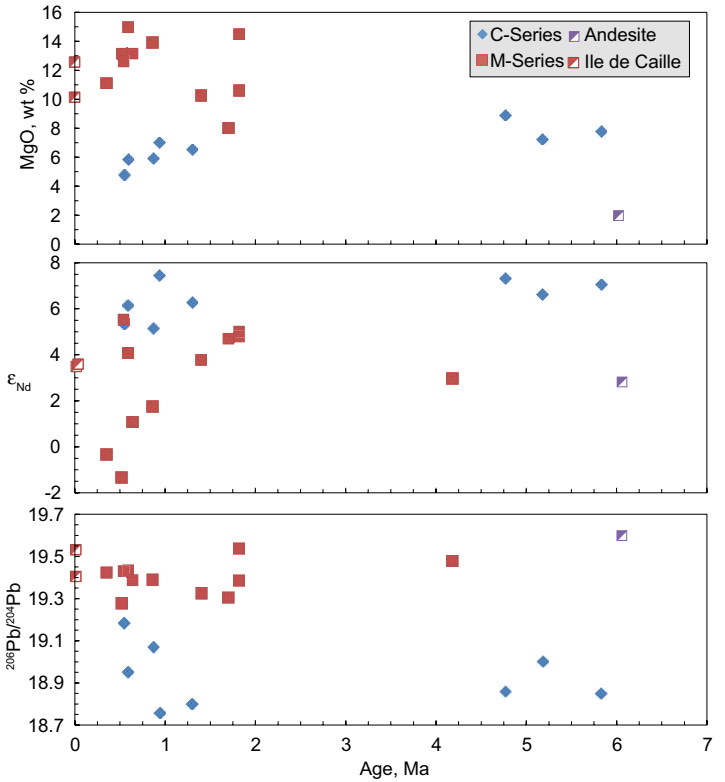

Figure 15. $^{206}Pb/^{204}Pb$, ε_{Nd}, and MgO as a function of age in Grenadian samples. Symbols are the same as in Figure 8.

This suggests the dike was produced by island-arc magmatism rather than backarc magmatism, which in turn suggests the southernmost part of the Lesser Antilles island arc has remained fixed on the leading edge of the Caribbean plate because it has moved slowly to the northeast since the Eocene, despite backarc spreading and a westward shift of the arc to the north.

Evolution of Grenadian C-Series Magmas

Devine (1995) previously discussed the evolution of M-series magmas included in our samples; here we focus primarily on the C series.

Stamper et al. (2014a) stated "MELTS modelling confirms experimental hypotheses that the two lava series can be derived from a common picritic magma" (p. 1353). We carried out numerous simulations with MELTS (Ghiorso and Gualda, 2015; Ghiorso and Sack, 1995; Ghiorso et al., 2002) under various

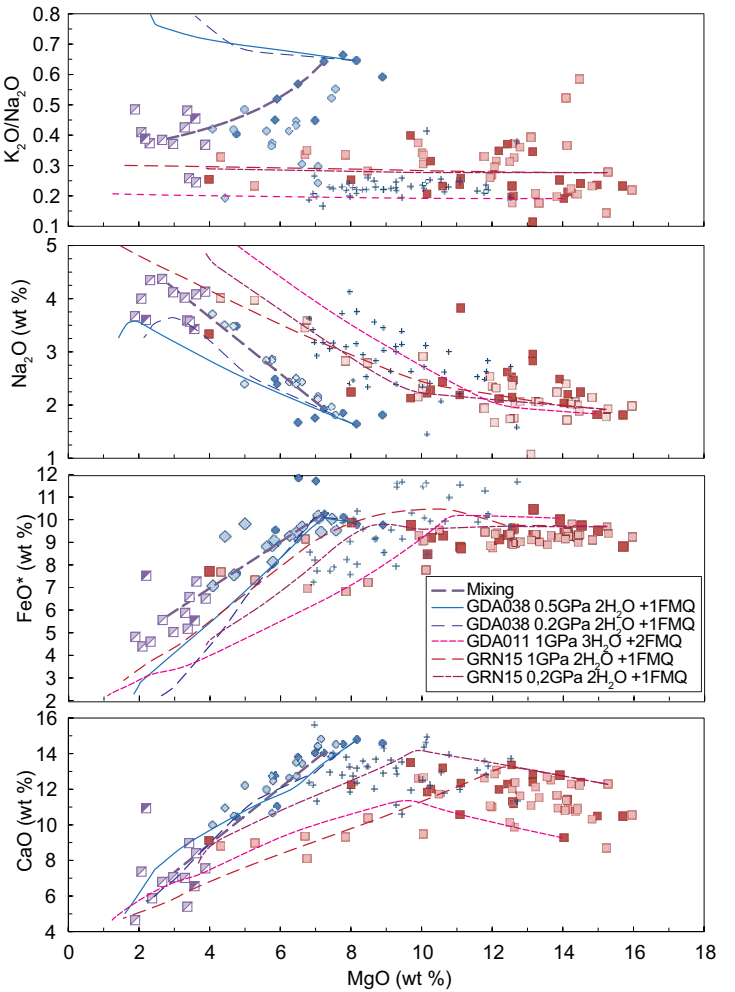

Figure 16. Comparison of fractional crystallization simulations and simple two-component magma mixing models of Grenadian magma evolution. Fractional crystallization models were performed with MELTS under stated conditions. For example, GDA038 0.5GPa 2 H_2O +1FMQ was performed with GDA038 as the parent crystallizing at 0.5 GPa pressure, 2% H_2O, and oxygen fugacity 1 unit above the fayalite-magnetite-quartz buffer. Dashed bold purple line illustrates mixing between C-series sample GDA038 and andesite 307 of Thirlwall et al. (1996). Solid bold purple line illustrates mixing between C-series sample GDA049 and andesite 100 of Thirlwall et al. (1996). (Isle de Caille samples are included with M series.)

assumptions of pressure, water content, and oxygen fugacity, some of which are shown in Figure 16. Simulations beginning with two primitive M-series compositions, GRN15, the sample experimentally studied by Stamper et al. (2014a), or our sample GDA011 (not shown), do a reasonably good job of reproducing major-element trends of the M series, particularly at pressures near 1 GPa, consistent with the inference of Stamper et al. (2014a) that these magmas equilibrated at these pressures. However, our best-fit models are those with lower oxygen fugacity (FMQ +1 to +2 and <Ni-NiO +2) than the oxygen fugacity (>Ni-NiO +3) inferred by Stamper et al. (2014a) from their experimental studies, and we are unsure why.

In contrast, no simulation we performed using a primitive M-series composition reproduced the CaO-MgO or Na_2O-MgO trend observed in the C series, nor do any of these models account for the high K_2O/Na_2O in the C series. As Thirlwall et al. (1996) pointed out, the clear distinctions in isotope and trace-element compositions of the two series, particularly in the more primitive members, require that C- and M-series magmas be derived from distinct sources in the upper mantle, and our MELTS simulations are consistent with that conclusion. Models beginning with magnesian C-series basalt, such as GDA038GM, well reproduce major-element trends of the C series. We used this composition, the separated groundmass of a cpx-bearing mafic (>8% MgO) basalt, for many of our simulations because it should approximate a liquid composition. Those simulations with relatively low oxygen fugacity of FMQ +1, several percent water, and pressures ranging from 0.2 to 0.5 GPa were most successful (Fig. 16).

However, all of these models predict that K_2O/Na_2O and Sr should increase with decreasing MgO, whereas the opposite occurs in the C series (Figs. 16 and 17). In particular, plagioclase fractionation is the only way Sr concentrations can decrease, and our MELTS simulations show plagioclase is typically a late-crystallizing phase, not precipitating until MgO falls below ~4%, which is consistent with its rarity as a phenocryst phase in the C series. The only way K_2O/Na_2O could decrease during fractional crystallization is through fractionation of biotite or phlogopite. We have observed biotite and phlogopite as a groundmass phase in some samples (although it is not clear that these phrases are primary), and small amounts of biotite do appear in our MELTS simulations at temperatures below 1000 °C. However, the amounts are markedly insufficient to account for the decrease in K_2O/Na_2O. Finally, fractional crystallization alone cannot explain the change in radiogenic-isotope ratios with MgO shown in Figure 18.

Assimilation or Magma Mixing?

On the basis of correlations between major elements and radiogenic-isotope ratios, Thirlwall and Graham (1984) argued that fractional crystallization of C-series lavas was "accompanied by assimilation of sedimentary material from the island arc crust" (p. 427). Thirlwall et al. (1996) further argued that correlations between $\delta^{18}O$ and radiogenic-isotope ratios indicated that both series had assimilated sediment.

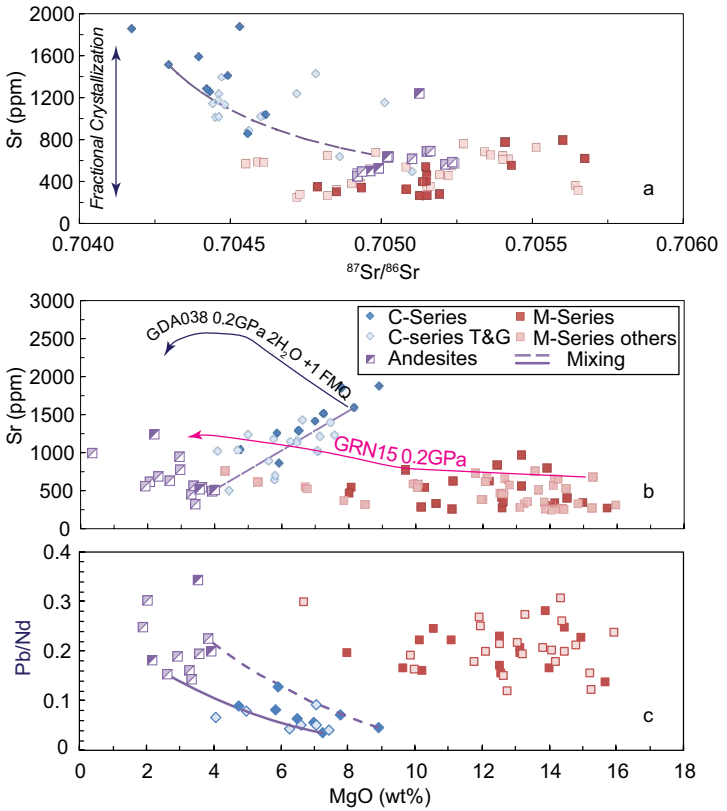

Figure 17. (A) and (B) Comparison of MELTS fractional crystallization models of M-series sample GDN015 and C-series sample GDA038, both at 0.2 GPa with 2% H_2O and oxygen fugacity 1 log unit above the fayalite-magnetite-quartz (FMQ) buffer, versus mixing between C-series sample GDA038 and andesite 307 of Thirlwall et al. (1996) (dashed purple line) to explain the variation in Sr and $^{87}Sr/^{87}Sr$ with MgO in C-series magmas. Fractional crystallization should not change the $^{87}Sr/^{86}Sr$ ratio. (C) Pb/Nd variation with MgO and mixing between C-series basalt GDA049 and andesite sample 100 of Thirlwall et al. (1996) (dashed line) and between C-series basalt GDA005 and andesite sample 307 of Thirlwall et al. (1996). Symbols are the same as in Figure 8, except that Isle de Caille samples are included with M series.

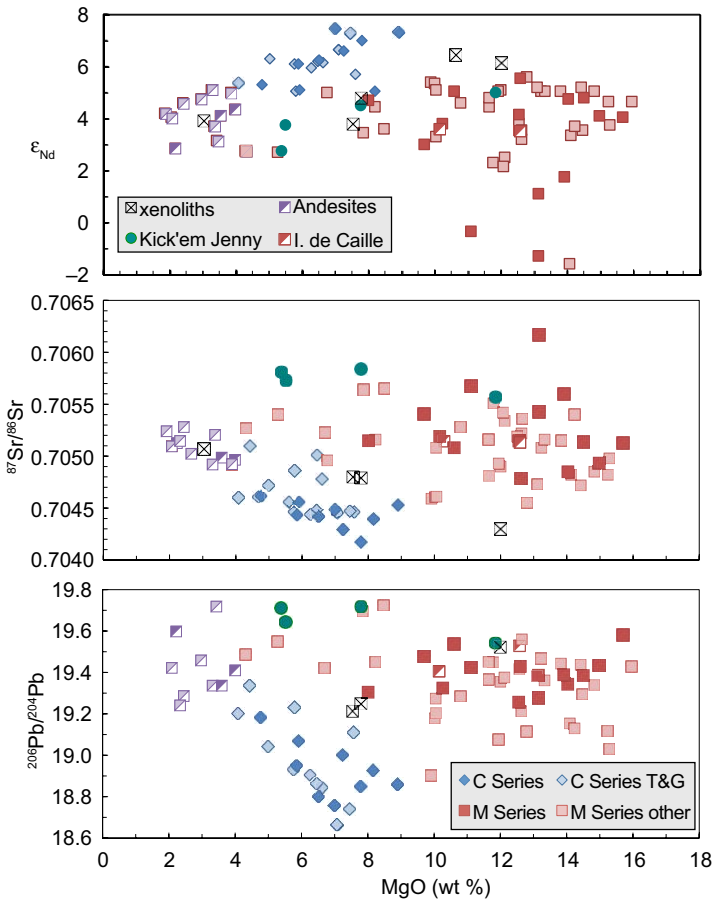

Figure 18. Strontium-, Nd-, and Pb-isotope ratios as a function of MgO in Grenada samples. Symbols and data sources are the same as Figure 8, except Isle de Caille samples, which are included with M series. Correlations between isotope ratios and MgO are statistically significant in the C series but not in the M series.

We observe strong correlations between radiogenic-isotope ratios and MgO in the C series (Fig. 18); all correlations between radiogenic-isotope ratios (including with $^{207}Pb/^{204}Pb$ and $^{208}Pb/^{204}Pb$ not shown) and MgO in the C series are statistically significant at the 0.5% level (i.e., there is a 0.5% chance they are merely random). Although there may appear to be trends of isotope ratios varying with MgO in the M series, only $^{206}Pb/^{204}Pb$ correlates significantly with MgO and only at the 5% significance level; other isotope ratios, including $^{207}Pb/^{204}Pb$ and $^{208}Pb/^{204}Pb$, do not correlate significantly with MgO.

We agree with Thirlwall and Graham (1984) that evolution of C-series magmas cannot be explained by fractional crystallization alone. The isotopic disequilibrium we observe in GDA038 also cannot be explained by fractional crystallization. However, we argue here that sediment assimilation also fails to explain C-series trends. Instead, mixing with evolved M-series melts stored in the arc crust and/or assimilation of M-series crystallization products provides the best explanation. Several quite strong lines of evidence support this hypothesis.

- The sedimentary rocks that do outcrop on Grenada, the Tufton Hall Formation, are not an appropriate assimilant, as Thirlwall and Graham (1984) and Thirlwall et al. (1996) pointed out. Their isotopic composition is not appropriate (Figs. 12–14). Furthermore, its REE pattern shows a very strong negative Ce anomaly such that the amount of Tufton Hall Formation that would have to be assimilated to explain the decrease in ε_{Nd} in the C series would also produce Ce anomalies in the lavas, and we find none (Fig. 10).
- Thirlwall et al. (1996) found that $\delta^{18}O$ in clinopyroxenes from C-series lavas ranged from typical mantle values of ~+5.5‰ to as high as +6.59‰ and argued that this provided additional evidence of sediment assimilation by C series. However, these $\delta^{18}O_{cpx}$ values do not correlate with MgO (r = 0.14). Thirlwall et al. (1996) reported that "Samples with higher $^{206}Pb/^{204}Pb$ and lower ε_{Nd}, except sample number 6073, generally have higher $\delta^{18}O_{cpx}$ values" (p. 4794). However, all correlation coefficients between $\delta^{18}O_{cpx}$ and radiogenic-isotope ratios are below statistical significance. Indeed, the only statistically significant correlation of $\delta^{18}O_{cpx}$ is with $\delta^{18}O$ of the whole rock. As Thirlwall et al. (1996) noted, the latter correlate with loss on ignition and undoubtedly have been disturbed by tropical weathering. These correlations between $\delta^{18}O$ in whole rocks and clinopyroxene and loss on ignition suggest that oxygen-isotope ratios in clinopyroxene have also been affected by weathering.
- Sediments usually have relatively high K_2O/Na_2O ratios. For example, in Plank's (2014) compilation of sediment subducting beneath the Southern Lesser Antilles $K_2O/Na_2O = 0.72$, it is even higher, 0.88, in her global average of subducting sediment (GLOSS II). Thus, in most instances, assimilation of sediment should lead to increasing K_2O/Na_2O; yet it clearly decreases with decreasing MgO in C-series lavas (Fig. 16). Because simple fractional crystallization also produces increasing K_2O/Na_2O with decreasing MgO (Fig. 16), the K_2O/Na_2O-MgO relationship provides compelling evidence of mixing or assimilation but equally compelling evidence that the assimilant must have low K_2O/Na_2O, effectively ruling out sediment.
- As we pointed out earlier, the C-series and M-series arrays converge at low MgO, and this is true of isotope ratios and trace elements as well as major elements. This seems unlikely to be coincidental and is exactly what would be expected if C-series magmas were mixing with or assimilating evolved M-series material. This possibility is supported by the observation that eruption of C-series and M-series lavas has been thoroughly intermingled in both space and time, indicating both magma series utilize the same crustal plumbing system.
- Thirlwall et al. (1996) rejected the possibility that C-series evolution could be explained by assimilation or mixing with M-series material on the basis that "Pb/Nd ratios in most M-series lavas are too high" to generate the C-series trajectory. In fact, Pb/Nd ratios in C-series lavas are readily explained by mixing between C-series basalts and evolved andesites with M-series Pb/Nd ratios, as Figure 17C illustrates.

It is more difficult to decide whether C-series magmas are mixing with M-series liquids stored in the shallow crust or assimilating their crystallization products. The metamorphic xenoliths we collected and analyzed are amphibolite-facies and pyroxene-hornfels–facies rocks. We interpret them to be crustal intrusive rocks that were contact metamorphosed in the vicinity of crustal magma reservoirs before being carried to the surface by erupting magma. Although a range of compositions is observed, most of the xenoliths are too aluminous to be potential assimilants in AFC processes, although some are high in CaO and have low $^{87}Sr/^{86}Sr$ ratios. Their $^{206}Pb/^{204}Pb$ ratios, however, are all higher than those of C-series basalts. The cumulus-textured xenoliths are both low in SiO_2 and high in CaO, but their Sr contents are all too low to account for the high Sr contents of C-series basalts by bulk assimilation, and their $^{87}Sr/^{86}Sr$ and $^{206}Pb/^{204}Pb$ ratios are all higher than those of C-series basalts.

In short, none of the xenoliths analyzed to date has the unique combination of characteristics inferred for bulk assimilants in AFC processes. Furthermore, a simple magma mixing model between somewhat evolved C-series compositions such as GDA049 (7% MgO) and M-series andesites such as Thirlwall et al.'s (1996) sample 100 (2.7% MgO) well reproduces both major-element, Sr, and $^{87}Sr/^{86}Sr$ trends in Figures 16 and 17. Based on these observations, we favor simple magma mixing but acknowledge that assimilation of igneous or metaigneous rocks within the arc crust may also occur, as Reubi et al. (2011) have argued occur beneath Volcan Llaima in Chile. Indeed, as Devine and Sigurdsson (1995) and Huang et al. (2011) have inferred this process to occur beneath Kick 'em Jenny, it may well occur beneath Grenada as well.

We also point out that although magma mixing does not consume energy in the form of latent heat of fusion as assimilation does, crystallization will nonetheless be induced when a basaltic magma mixes with a cooler, more evolved andesitic magma. Thus, fractional crystallization will proceed simultaneously with magma mixing, and the trends produced will in some cases be indistinguishable from those produced by either AFC or fractional crystallization alone.

Thirlwall et al. (1996) also argued that an M-series subset, the low-La/Y–evolved samples, had assimilated sediment within the crust. They reported two M-series samples contained quartz xenocrysts with $\delta^{18}O$ values of +9.5‰ and +10‰. The presence of quartz, which is not a crystallizing phase in these lavas, is certainly evidence of assimilation. The elevated $\delta^{18}O$ values indicate the quartz is derived from material that had interacted with water at low temperature. Sediment is a clear possibility, although altered silicic igneous rock may be another. These two samples, along with sample 310A of Thirlwall et al. (1996), have the highest $^{206}Pb/^{204}Pb$ of all Grenadian lavas and also rather high $^{87}Sr/^{86}Sr$, but their ε_{Nd} falls in the middle of the M-series range. Assimilation of Tufton Hall Formation rocks cannot explain their isotopic compositions, however, because their Pb and Sr isotope ratios are higher than those of the Tufton Hall. While these lavas have certainly assimilated some crustal material, the nature of that material and its effect on magma composition, particularly radiogenic-isotope ratios, can only be speculated upon.

As Thirlwall et al. (1996) noted, sediments from Ocean Drilling Program (ODP) Site 543 on the subducting Atlantic plate analyzed by White et al. (1985) had $^{206}Pb/^{204}Pb$ too low and $^{208}Pb/^{204}Pb$ and $^{207}Pb/^{204}Pb$ too high to explain the most extreme Pb isotopic compositions observed in the M series. They also noted that no sediment from the Caribbean plate has Pb-isotope ratios as high as these samples, stating, "No constraint is thus provided by Pb on whether the high $^{206}Pb/^{204}Pb$ component is derived from sediment in the subduction zone or the arc crust" (p. 4803). They chose nonetheless to conclude that the high $^{206}Pb/^{204}Pb$ component of these samples was acquired through assimilation.

Subsequently, however, Carpentier et al. (2008) reported very radiogenic Pb, with $^{206}Pb/^{204}Pb$ up to 27.69, from ODP Site 144 located on the Demerara Rise to the southeast of Grenada. The radiogenic Pb occurs in black shales deposited during ocean anoxia event OAE3 at 93–96 Ma, and the radiogenic nature results from the relatively U-rich nature of these black shales and its radiogenic decay since deposition. Consequently, $^{207}Pb/^{204}Pb$ and $^{208}Pb/^{204}Pb$ are not elevated and, as Carpentier et al. (2008) point out, mixing of this material with more typical Pb-isotope ratios of sediments in the region produces Pb-isotope ratios that can explain all Pb isotopic compositions observed in Grenadian magmas (figure 6 of Carpentier et al., 2008). Black shales associated with anoxia event OAE3 occur broadly across the Atlantic on crust of approximately the same age, including crust subducting beneath the southern Lesser Antilles. The age of the Atlantic crust subducting beneath the Lesser Antilles decreases northward, so that this black shale unit does not occur at Site 543, which drilled into 91 Ma crust. The lower Pb-isotope ratios observed in the northern part of the Lesser Antilles arc (White and Dupré, 1986) may thus reflect the absence of this black shale unit in the subducting sediment (Carpentier et al., 2008).

Thus, while these low-La/Y–evolved M-series magmas may have experienced assimilation, the effects of this on isotopic composition are uncertain. Carpentier et al. (2008) have shown that subducted sediment can explain their isotopic composition; in contrast, whether sediment that could also explain their isotopic compositions is present in the Grenadian arc crust remains speculative. Regardless, the general lack of statistically significant correlations between MgO and isotope ratios (except $^{206}Pb/^{204}Pb$ as noted above) in the M series suggests that sediment assimilation is not an important control on M-series evolution. Furthermore, the evolution of the M series is reasonably well reproduced by MELTS simulations—ours as well as those of Stamper et al. (2014a). We conclude that although some sediment assimilation may occur, its effects are secondary, contributing to magma heterogeneity, and do not explain the principal compositional features of Grenadian magmas.

The obvious question then is why does magma mixing (or assimilation of igneous crust) exert strong control on the evolution of C-series compositions without also affecting the M series? We argue that it does affect the M series but less systematically with less obvious effect. The following observations support this inference:

- There are only a third as many analyses of C-series (26) as M-series (75) analyses in our database, suggesting the Grenadian crust consists dominantly of M-series material. Furthermore, xenoliths we analyzed have predominately M-series isotopic compositions, and most of the melt inclusions analyzed by Bouvier et al. (2010) appear to be M-series related. (It could be argued that the melt inclusions are M series only because the host lava is also, but the inclusions display considerable heterogeneity and appear largely unrelated to the host lava.) M-series magmas rising through the crust thus most commonly come in contact with M-series residual liquids and crystallization products. For the M-series, the effects of assimilation or mixing with this material would be difficult to distinguish from fractional crystallization alone.
- Second, M-series compositions are far more heterogeneous than C-series compositions in major and trace elements and isotopic compositions, and Thirlwall et al. (1996) and Woodland et al. (2002) identify some M-series samples with C-series affinities. We suggest that this M-series heterogeneity in part reflects occasional mixing with C-series magmas. Beyond that, the M-series heterogeneity makes assimilation or mixing more difficult to recognize.
- M-series compositions are somewhat bimodal; roughly 65% of reported analyses have MgO >12% with a second peak in abundance of ~4% MgO. The relatively primitive MgO-rich magmas have likely risen rapidly through the crust (some contain peridotite and harzburgite xenoliths) with relatively little opportunity for mixing or assimilation. Interestingly, Grenadian andesites are much more homogeneous than the basalts of either series, suggesting the former have been homogenized in crustal magma chambers, while the latter have not. As we noted earlier, andesite isotopic compositions fall within the range of M-series basalts, and hence they are most likely primarily derived from M-series parents. However, they may well have mixed with limited volumes of C-series magmas before homogenization. This mixing would explain the observation we made earlier, that it is not possible to distinguish between M series and C series below ~4%–6% MgO.

We suggest that magmas rising through volcanic plumbing systems everywhere frequently mix with residual liquids trapped in the crust or assimilate crystallization products of earlier magmas. Boron-isotope (Chaussidon and Jambon, 1994), chlorine-isotope (Bonifacie et al., 2008), and osmium-isotope (Gannoun et al., 2007) ratios in mid-ocean ridge basalts suggest assimilation of hydrothermally altered crust is common at mid-ocean ridges, but this is apparent only in these isotope ratios because of their extreme sensitivity to disturbance by hydrothermal alteration. The process is apparent in the Grenada C series because they are compositionally distinct from the M-series material that makes up most of the Grenadian crust. Because that crust consists of older lavas that may have weathered extensively before being buried and intrusive products subject to hydrothermal alteration, the oxygen-isotope ratios in the crust may vary from below to above the mantle

value, and assimilation of this material may, in part, contribute to oxygen isotopic heterogeneity.

Strong cases for sediment assimilation have been made elsewhere is the Lesser Antilles, where far more extreme radiogenic- and oxygen-isotope ratios have been documented in andesites and dacites of Martinique and St. Lucia (Bezard et al., 2014; Davidson and Harmon, 1989), although alternative explanations have been proposed (e.g., Labanieh et al., 2010), and, again, quartz xenocrysts in the some Grenadian lavas also document assimilation. We do not argue that sediment assimilation never occurs in the Lesser Antilles—only that it is a secondary process on Grenada, and it clearly fails to explain the trends observed in the C series. We strongly disagree with the extreme statement of Bezard et al. (2014) that "assimilation seems to be responsible not only for the isotopic heterogeneity observed in St Lucia but also in the whole Lesser Antilles since St Lucia encompasses almost the whole-arc range of isotopic compositions" (p. 51). Unlike St. Lucia where extreme isotope ratios are restricted to highly evolved magmas, the most enriched Sr, Pb, and Nd isotopic signatures in Grenada occur in highly magnesian, primitive, and occasionally xenolith-bearing M-series basalts that have risen rapidly through the crust with no opportunity to assimilate sediments. Regardless of whether assimilation or magma mixing occurs in Grenada, we agree with Thirlwall and Graham (1984) and Thirlwall et al. (1996) that the range in isotopic compositions in magmas is inherited principally from the mantle sources.

Generation of C- and M-Series Magmas

Distinct magma series in island-arc volcanoes are well known, but both the Grenadian series are relatively uncommon in their nominally alkalic character, in contrast to tholeiitic or calc-alkaline magmas that dominate in this environment (Miyashiro, 1974). The M series is also highly unusual in that it includes quite mafic, peridotite xenolith-bearing members, whereas evolved compositions typically predominate on most other island-arc volcanoes, including those of the Lesser Antilles.

As Devine (1995) noted, the major-element composition of the most mafic members of the M series are "very similar in composition to those of high-pressure (20-30 kb) experimental batch partial melts of mantle peridotite" (p. 8). Stamper et al. (2014b) reached similar conclusions with the additional constraint that the M series was apparently generated under hydrous, oxidizing conditions. Thirlwall et al. (1996) concluded that the compositions of M-series samples with the least radiogenic Nd were "consistent with generation from a mantle source with a relatively high contribution (~2%) from subducted local seafloor sediment." What, however, are the details of magma generation beneath Grenada? Can subducted sediment also explain the trace-element patterns observed in these lavas?

A first question would be: What is the nature of the C-series magma source: is it peridotite or pyroxenite? C-series magmas are unusual in a subduction zone setting, not only in their silica-undersaturated nature, a feature shared with many M-series lavas, but also in their high CaO content and high CaO/Al_2O_3 ratios (as high as 0.99). Although such compositions are unusual, they are not unique. Because clinopyroxene is the principal host mineral for calcium in the upper mantle, this logically leads to the suspicion that such magmas might be melts of pyroxenite rather than peridotite; this could potentially also explain why more magnesian C-series magmas are not found (Parkinson et al., 2003). Schiano et al. (2000) argued that CaO-rich nepheline-normative magmas from Batan, Philippines, were melts of pyroxene-rich cumulates in the lower crust or shallow upper mantle. Médard et al. (2004) and Elburg et al. (2007), among others, have arrived at similar interpretations for CaO-rich, silica-undersaturated magmas in other island arcs. However, the compositions considered in those studies were richer in CaO (>15%), had $CaO/Al_2O_3 > 1$, and were generally poorer in silica than the C series considered here.

Sorbadere et al. (2012) considered the compositions of MgO-rich melt inclusions in nepheline-normative arc magmas, including those from Grenada analyzed by Bouvier et al. (2010), and they found that their compositions defined trends suggestive of mixing between melts generated by partial melting of peridotite- and amphibole-bearing, clinopyroxene-rich lithologies. This is illustrated in Figure 19 in two ternary projections in which compositions are recast into the system $CaO-MgO-Al_2O_3-SiO_2$ (CMAS) using the method of O'Hara (1968). The melt inclusions (black dots) trend toward or lie within the field of experimental amphibole-bearing clinopyroxenite melts at lower-crustal to shallow-mantle pressures. Such lithologies are included in xenoliths found in Grenada (Arculus and Wills, 1980); so it is certainly plausible that partial melts of these cumulates have mixed with Grenadian magmas. It is also consistent with assimilation of amphibole-bearing assemblages that appears to occur in Kick 'em Jenny (Devine and Sigurdsson, 1995; Huang et al., 2011). In contrast, however, the least fractionated members of the C and M series plot within the field of experimental peridotite melts. (Some M-series compositions plot outside of the field shown, which is for anhydrous melting, but within the field for hydrous peridotite melting.) In particular, C-series magmas show no obvious trend toward the pyroxenite field, nor does the M series. Although none of the C-series compositions may be primary magmas, fractional crystallization would tend to move compositions away from, not toward, the amphibole-bearing clinopyroxenite field. Furthermore, the liquidus temperature of GDA038GM calculated with MELTS is 1133° to 1256 °C assuming 3% water and mid-crustal to shallow-mantle pressures (0.2–1 GPa), hot enough to produce extensive melting in the region, for which there is no seismic evidence.

Although neither the C nor M series appear to be pure clinopyroxenite melts, Sorbadere et al. (2013) showed that under hydrous melting conditions, melting of mixed pyroxenite-peridotite lithologies or mixtures of melts produced separately from each can be difficult to distinguish from purely peridotite melts. We conclude that melting of a peridotite source has generated the C series, but we cannot say the source is exclusively peridotite, and we cannot rule out the possibility that their silica-undersaturated, CaO-rich nature results from a contribution from pyroxenite melting. Based on observations on Grenadian peridotite xenoliths, Parkinson et al. (2003) have suggested that

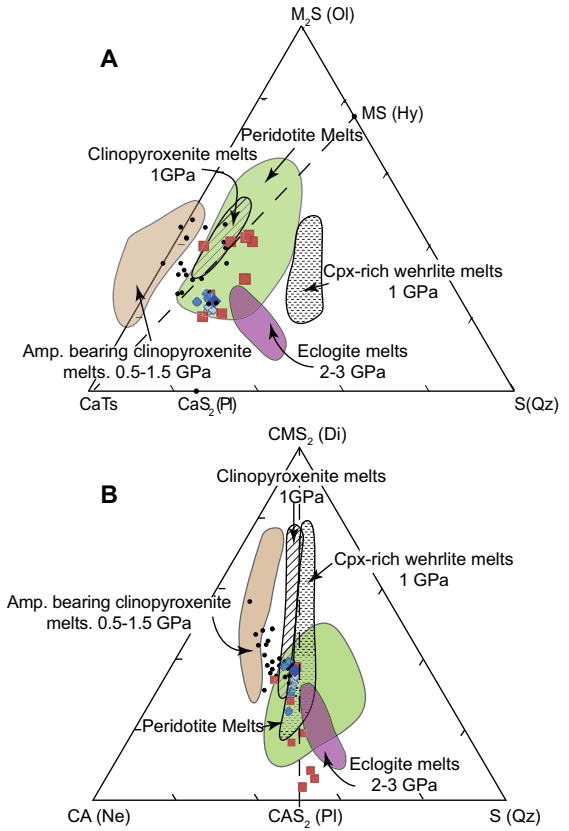

Figure 19. Compositions of least fractionated C-series (blue diamonds) and M-series (red squares) basalts and melt inclusions of Bouvier et al. (2010) (black dots) recast in the system CaO-MgO-Al_2O_3-SiO_2 (CMAS) of O'Hara (1968) and compared with the fields for pyroxenite, eclogite, and peridotite melts. Larger, darker triangle is GM038GM. (A) Projection onto the *molar* M_2S–CAS-S plane (corresponding to components olivine-Ca-Tschermack-quartz) from CMS_2 (diopside). (B) Projection onto the *molar* CA (nepheline)–CMS_2 (diopside)–S (quartz) plane. Both C- and M-series plot within the field of peridotite melts (the latter when hydrous melting is considered). Fields are from Sorbadere et al. (2012). Projections computed with the software of France and Nicollet (2010).

clinopyroxene-rich lithologies could develop through melts reacting with harzburgite that in turn could serve as a source for the C series. We certainly cannot rule out such a scenario, but we would point out that radiogenic-isotope ratios preclude the melts reacting with the harzburgite being related to the M series; instead they would have to be from earlier episodes of magmatism, perhaps during backarc spreading. In the following, we assume that both the C series and M series are generated by melting of peridotite within the mantle wedge.

Subducted oceanic crust and sediment experience dehydration and partial melting, and these fluids then metasomatize the mantle wedge, where the subduction-related magmas are generated (e.g., Kelemen et al., 2014; Tatsumi and Kogiso, 2003). In view of that, we attempted to model the genesis of Grenadian M- and C-series lavas with a two-stage model in which a melt of a mixture of oceanic crust plus sediment or a hydrous fluid produced by dehydration of this mixture mixes with the overlying mantle wedge. The mixture then melts to produce the Grenadian magmas. As targets for modeling, we chose M-series sample GDA138, which has a composition close to that expected of a primary mantle peridotite melt (~15% MgO and Mg# >72) as representative of parental M-series magmas. As the most mafic C-series composition, GDA005 was chosen as the C-series target. Its composition, 8.9% MgO and Mg# ≈0.68, indicates it is unlikely to be a primary melt of mantle peridotite and thus likely experienced some fractional crystallization, but the effect of this is very much second order compared to mixing and melting effects. In the model, we assume the sediments have the composition of Southern Lesser Antilles subducting sediment (SLASS) of Plank (2014), and basaltic oceanic crust has the trace-element and isotopic composition of average MORB in White and Klein (2014) but with a somewhat higher $^{87}Sr/^{86}Sr$ (0.7043) due to seawater alteration. We assume that the mantle wedge has the depleted mantle composition of Salters and Stracke (2004).

In both the melting and dehydration models, we first attempted to reproduce isotope ratios through balancing the three components: sediment, oceanic crust, and depleted mantle. Of these, Nd-isotope ratios are particularly useful in assessing the sediment contribution, since the Nd isotopic compositions of oceanic crust and depleted mantle are similar; but sediment is quite different. Because of alteration, Sr isotopes are likely to be different in the oceanic crust than depleted mantle, thus it is useful in assessing the oceanic crust contribution once the sediment contribution is determined. Lead isotopes are highly heterogeneous in Lesser Antilles sediment (Carpentier et al., 2008; White et al., 1985) and, hence, provide poorer constraints than Nd- and Sr-isotope ratios.

For the dehydration models, we used trace-element, fluid-mobility factors determined by Kessel et al. (2005) at 800 °C and 4 GPa, which are close to slab condition beneath the arc estimated by Syracuse et al. (2010). For dehydration models, we assumed coesite-eclogite phase proportions with up to several percent rutile based on the experiments of Schmidt et al. (2004) at these temperatures and pressures and adopted the garnet and clinopyroxene partition coefficients of Zack et al. (1997). We varied the extent of fluid released, the extent of partial melting in both the slab and mantle wedge, and the amount of fluid or melt added to the mantle wedge to try to duplicate trace-element patterns of the two target compositions. Results are illustrated in Figure 20.

For both the C and M series, dehydration models could not reproduce observed Sr and Nd isotopic compositions because the high fluid mobility of Sr relative to Nd results in either $^{87}Sr/^{86}Sr$ or ε_{Nd} too high for any combination of components. Dehydration models also tended to overpredict the abundance of fluid-mobile elements such as Rb, K, U, and Pb and underpredict the abun-

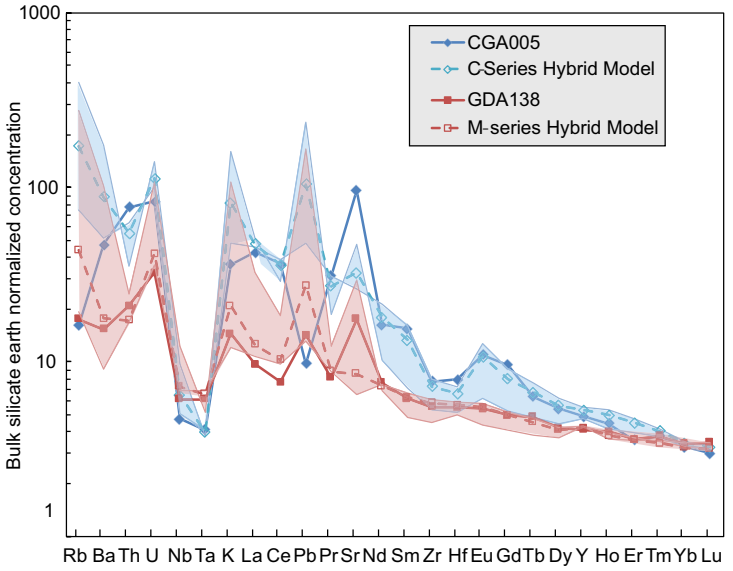

Figure 20. Comparison of a two-stage model for magma generation beneath Grenada with the incompatible-element concentrations in representative C-series (GDA005) and M-series (GDA138) magmas (solid lines). In the model, a mixture of oceanic crust plus sediment melts and/or dehydrates to produce a hydrous fluid that then mixes with the overlying peridotite mantle wedge. The wedge then melts to produce Grenadian magmas. The fields show the range from pure hydrous fluid (with 2% and 2.5% fluid added to the wedge for the C- and M-series, respectively) to pure melt end-members of this model (4% of slab melt for both series). Dashed lines show the best-fit hybrid models, in which the magmas are generated by melting of depleted mantle wedge, which is a mixture of these pure fluid- and pure melt-metasomatism models (30% fluid for the C series; 12% for the M series). Fluid-mobility factors were taken from Kessel et al. (2005), slab phase proportions from Schmidt et al. (2004), and partition coefficients from Zack et al. (1997). The sediment is to have the composition of the Southern Lesser Antilles subducting sediment (SLASS) average of Plank (2014) and oceanic crust to have the composition of average mid-ocean ridge basalts (MORBs) of White and Klein (2014). The sediment contribution is 10% to the fluid and 5% to the slab melt for the C-series model and 16% for both fluid and melt for the M-series model. The mantle wedge is assumed to have the composition of Salters and Stracke (2004), and the extent of mantle wedge melting is 8% for the C series and 25% for the M series in all cases.

dance of the less fluid-mobile elements. Melting models were somewhat more successful in matching Sr and Nd isotopic compositions, but, converse to dehydration models, resulted in either $^{87}Sr/^{86}Sr$ ratio or ε_{Nd} too low and, as might be expected, underpredicted the abundance of fluid-mobile elements.

The most successful models were "hybrid" ones in which incompatible elements were added from the slab to the mantle wedge in both hydrous fluids and partial melts. These could approximately predict both Sr- and Nd-isotope ratios in both our C- and M-series targets. For example, the hybrid C-series model shown in Figure 20 predicts $^{87}Sr/^{86}Sr$ and ε_{Nd} of 0.70451 and +6.5 compared to the values for GDA005 of 0.70450 and 6.2, respectively. The M-series hybrid model predicts $^{87}Sr/^{86}Sr$ and ε_{Nd} of 0.70481 and +3.6 compared to the values for GDA138 of 0.704930 and +3.6, respectively. As Figure 20 shows, these models approximately match the less mobile trace elements of these two lavas; mobile elements are less well matched, most significantly for Sr and Pb. None of our models are able to reproduce the very high Sr/Pb ratios observed in the C series; this unusual feature of C-series magmas remains problematic. Rapid breakdown of a Sr-rich mineral such as lawsonite might produce a particularly Sr-rich (and perhaps Ca-rich as well) fluid, but this fluid should also be Pb rich (e.g., Martin et al., 2014). One can only speculate that Pb had either been lost from the slab during early stages of subduction or is retained in some accessory phase. Rb and K are also poorly matched in the C-series model (however, it should be noted that GDA005 is substantially poorer in Rb than most other C-series lavas). There are a variety of possible explanations for the mismatches. Among these, our model, based on batch dehydration or batch melting, is overly simplistic, and some of our assumptions about mineralogy and partition coefficients may be inaccurate; however, another important factor is the heterogeneous nature of the sediment being subducted beneath the Lesser Antilles.

Nevertheless, it appears possible to draw the following broad inferences:

- Sediment contributes significantly more to the M series than the C series. In our model, the total mass contribution of sediment (via melts and hydrous fluids) to the M-series lava GDA138 is 0.6%; the contribution for the C-series lava GDA005 is 0.2%. However, GDA138 has less radiogenic Sr and Pb and more radiogenic Nd than many other M-series lavas, implying significantly larger sediment contributions to those other M-series magmas, perhaps as much as the 2% estimated by Thirlwall et al. (1996).
- Both fluids and melts appear to be involved in modifying mantle-wedge composition to produce Grenadian magmas.
- The fluid contribution is less for the M series than for the C series. Our hybrid model for the M-series source consists of 12% fluid-metasomatized mantle wedge (and 88% melt metasomatized) compared to 30% fluid-metasomatized mantle wedge for the C series.
- Melts thus appear to be the predominant carrier of incompatible elements from the slab to the mantle wedge beneath Grenada. Syracuse et al. (2010) estimated the slab-top temperature beneath the Southern Lesser Antilles as between 793 °C and 823 °C. The higher temperature would be close to the wet solidus, which is bracketed by experiments of Schmidt et al. (2004) between 790 °C and 850 °C. Our results suggest that melting occurs and, consequently, that either actual temperatures are at or above the high estimate of Syracuse et al. (2010), or the slab-top solidus is near the low end of this range.
- Larger melt fractions are involved in generation of M-series magmas, both in the slab and in the mantle wedge, than in generation of C-series magmas, consistent with the inference of Thirlwall et al. (1996). For example, in the hybrid models shown in Figure 20, the C series is generated by 8% melting of the mantle wedge, while the M series is generated by

25% melting. Of course, these values are model dependent, but they are consistent with the highly magnesian character of parental M-series magmas and less magnesian character of the least evolved C-series magmas. On the whole, smaller melt fractions, a source metasomatized by proportionally less melt, and more fluid are consistent in suggesting C-series magmas are generated under cooler conditions than are the M series.

- Finally, the quite moderate slope of rare-earth patterns in both the M and the C series requires that garnet is absent or nearly so in residues of mantle-wedge melting. This could be because melting occurs at pressures below the stability field of garnet, garnet is exhausted before melting is complete, or that garnet was consumed in previous melting episodes of the mantle wedge.

CONCLUSIONS

The chemistry of a basalt that we analyzed from Mayreau is consistent with its formation in a backarc spreading environment and consistent with the conclusion of Speed et al. (1993) that the Grenadine Plateau consists of uplifted crust formed by backarc spreading in the Eocene. This same crust likely underlies much of the Southern Lesser Antilles island arc. Union Island consists of supra-subduction zone igneous rocks that erupted between 6.5 and 3 million years ago with chemistry intermediate between that of the C and M series of Grenada, although they are on average more differentiated than the Grenadian lavas, and highly magnesian lavas are lacking.

Based on our $^{40}Ar/^{39}Ar$ age of a dacitic dike intruding the Eocene Tufton Hall Formation sedimentary rocks, it appears that supra-subduction volcanism was occurring in the vicinity of Grenada since at least 38 Ma. However, our new $^{40}Ar/^{39}Ar$ ages reveal that the present volcanic edifice of Grenada has been constructed only over the past 6 million years. Previously published K-Ar ages indicating a longer time span are in error.

Over this period, C- and M-series lavas have erupted from the same centers on the island, implying they utilize the same crustal plumbing system. Both are generated within a mantle wedge that has been metasomatized by both hydrous fluids and melts from the subducting oceanic crust and sediment. Hydrous fluids are more important in modifying the C-series source than the M-series source, but melts nevertheless are the more important metasomatizing agent in both cases, implying the slab melts beneath the Southern Lesser Antilles.

The most primitive M-series magmas contain only microphyric olivine, and approximate primary peridotite melts formed at depths of 40–90 km. They appear to have formed by large extents of melting (~25%) and have ascended rapidly without having re-equilibrated with the crust and upper mantle through which they passed. The incompatible-element abundances and isotopic compositions of these mafic M-series magmas require addition of ≥0.6% subducting sediment (SLASS; Plank, 2014) to the M-series source. The presence of Cretaceous U-rich black shales (Carpentier et al., 2008) explains the very high $^{206}Pb/^{204}Pb$ in some M-series lavas. In contrast to the M series, the contribution of subducted sediment to the C-series source is quite small: the addition of ~0.2% of Plank's (2014) SLASS to depleted mantle explains the Sr, Nd, and Pb compositions of the most primitive C-series lavas.

Compared with the M series, the most mafic C-series basalts are less magnesian (<9% MgO), Ca and Sr rich, and are exclusively nepheline normative, with olivine subordinate to clinopyroxene in size and abundance. They appear to have formed by significantly smaller melt fractions (~8%) than M-series lavas. Comparison with the experimental melts suggests C-series parents are primarily melts of peridotite, although in the C series, an admixture of a pyroxenite melt, particularly one of silica-poor clinopyroxenites, or melting of a mixed pyroxenite-peridotite source cannot be ruled out and may help to explain their CaO-rich, SiO_2-poor nature. If they are peridotite melts, then they must be the products of fractional crystallization of even more magnesian, olivine-bearing parental magmas not seen at the surface. Primary or near-primary parental magmas are often not found in island-arc volcanoes; the mystery in Grenada may be more the presence of near-primary M-series magmas than the absence of C-series primary magmas.

Both M- and C-series magmas do sometimes stagnate in the crust, where they evolve to andesitic compositions through fractional crystallization. This fractional crystallization is accompanied by magma mixing and perhaps also by assimilation through dissolution and reactive flow of magmatic cumulates. This magma mixing is most apparent in C-series evolution, in part because the M series dominates magmatism on Grenada and in part because the C-series parental magmas are much more homogeneous than those of the M series. Mixing with M-series magmas or assimilation of their crystallization products explains all aspects of C-series evolution: increasing Sr and Pb, decreasing Nd-isotope ratios, and decreasing Sr content and K_2O/Na_2O ratios. In contrast, none of these observations can be explained by the previously hypothesized sediment assimilation. Although some assimilation of sediments within the crust may occur in Grenada, its effect on magma compositions is at best secondary.

ACKNOWLEDGMENTS

This study was initiated and led by our colleague Joe Devine, who passed away suddenly in 2013. Joe completed his Ph.D. dissertation on the Lesser Antilles and spent much of his subsequent career studying volcanism in the Lesser Antilles, particularly Grenada. We greatly miss his company and the insights he brought to understanding the magmatic evolution in the Southern Lesser Antilles. This work was partially supported by National Science Foundation (grant EAR-9304102) to WMW and JDD and by a grant from the National Geographic Society to PC. We are grateful for careful reviews by Catherine Chauvel and Lucy McGee as well comments by guest editor Gray Bebout. These resulted in significant improvements in the manuscript.

REFERENCES CITED

Arculus, R.J., 1976, Geology and geochemistry of the alkali basalt—Andesite association of Grenada, Lesser Antilles island arc: Geological Society of America Bulletin, v. 87, no. 4, p. 612–624, doi:10.1130/0016-7606(1976)87<612:GAGOTA>2.0.CO;2.

Arculus, R.J., 1978, Mineralogy and petrology of Grenada, Lesser Antilles island arc: Contributions to Mineralogy and Petrology, v. 65, no. 4, p. 413–424, doi:10.1007/BF00372288.

Arculus, R.J., and Wills, K.J.A., 1980, The petrology of plutonic blocks and inclusion from the Lesser Antilles island arc: Journal of Petrology, v. 21, no. 4, p. 743–799, doi:10.1093/petrology/21.4.743.

Armstrong, R.L., 1971, Isotopic and chemical constraints on models of magma genesis in volcanic arcs: Earth and Planetary Science Letters, v. 12, no. 1, p. 137–142, doi:10.1016/0012-821X(71)90066-5.

Berggren, W.A., and Pearson, P.N., 2005, A revised tropical to subtropical Paleogene planktonic foraminiferal zonation: The Journal of Foraminiferal Research, v. 35, p. 279–298.

Bezard, R., Davidson, J.P., Turner, S., Macpherson, C.G., Lindsay, J.M., and Boyce, A.J., 2014, Assimilation of sediments embedded in the oceanic arc crust: Myth or reality?: Earth and Planetary Science Letters, v. 395, p. 51–60, doi:10.1016/j.epsl.2014.03.038.

Bonifacie, M., Jendrzejewski, N., Agrinier, P., Humler, E., Coleman, M., and Javoy, M., 2008, The chlorine isotope composition of Earth's mantle: Science, v. 319, no. 5869, p. 1518–1520, doi:10.1126/science.1150988.

Bouvier, A.S., Métrich, N., and Deloule, E., 2010, Light elements, volatiles, and stable isotopes in basaltic melt inclusions from Grenada, Lesser Antilles: Inferences for magma genesis: Geochemistry, Geophysics, Geosystems, v. 11, no. 9, Q09004, doi:10.1029/2010GC003051.

Briden, J.C., Rex, D.C., Faller, A.M., and Tomblin, J.F., 1979, K-Ar Geochronology and Palaeomagnetism of Volcanic Rocks in the Lesser Antilles Island Arc: Philosophical Transactions of the Royal Society of London A: Mathematical, Physical and Engineering Sciences, v. 291, no. 1383, p. 485–528, doi:10.1098/rsta.1979.0040.

Brown, G.M., Holland, J.G., Sigurdsson, H., Tomblin, J.F., and Arculus, R.J., 1977, Geochemistry of the Lesser Antilles volcanic island arc: Geochimica et Cosmochimica Acta, v. 41, no. 6, p. 785–801, doi:10.1016/0016-7037(77)90049-7.

Carpentier, M., Chauvel, C., and Mattielli, N., 2008, Pb-Nd isotopic constraints on sedimentary input into the Lesser Antilles arc system: Earth and Planetary Science Letters, v. 272, no. 1–2, p. 199–211, doi:10.1016/j.epsl.2008.04.036.

Chaussidon, M., and Jambon, A., 1994, Boron content and isotopic composition of oceanic basalts: Geochemical and cosmochemical implications: Earth and Planetary Science Letters, v. 121, no. 3–4, p. 277–291, doi:10.1016/0012-821X(94)90073-6.

Cheatham, M.M., Sangrey, W.F., and White, W.M., 1993, Sources of error in external calibration ICP-MS analysis of geological samples and an improved non-linear drift correction: Spectrochimica Acta, v. 48B, p. E487–E506.

Coler, D.G., Samson, S.D., and Speer, J.A., 1997, Nd and Sr isotopic constraints on the source of Alleghanian granites in the Raleigh metamorphic belt and Eastern slate belt, southern Appalachians, U.S: Chemical Geology, v. 134, no. 4, p. 257–275, doi:10.1016/S0009-2541(96)00063-0.

Davidson, J.P., and Harmon, R.S., 1989, Oxygen isotope constraints on the petrogenesis of volcanic arc magmas from Martinique, Lesser Antilles: Earth and Planetary Science Letters, v. 95, p. 255–270, doi:10.1016/0012-821X(89)90101-5.

Devine, J.D., 1995, Petrogenesis of the basalt-andesite-dacite association of Grenada, Lesser Antilles island arc, revisited: Journal of Volcanology and Geothermal Research, v. 69, no. 1–2, p. 1–33, doi:10.1016/0377-0273(95)00024-0.

Devine, J.D., and Sigurdsson, H., 1995, Petrology and eruption styles of Kick'em-Jenny submarine volcano, Lesser Antilles island arc: Journal of Volcanology and Geothermal Research, v. 69, no. 1–2, p. 35–58, doi:10.1016/0377-0273(95)00025-9.

Elburg, M.A., Kamenetsky, V.S., Foden, J.D., and Sobolev, A., 2007, The origin of medium-K ankaramitic arc magmas from Lombok (Sunda arc, Indonesia): Mineral and melt inclusion evidence: Chemical Geology, v. 240, no. 3–4, p. 260–279, doi:10.1016/j.chemgeo.2007.02.015.

France, L., and Nicollet, C., 2010, MetaRep, an extended CMAS 3D program to visualize mafic (CMAS, ACF-S, ACF-N) and pelitic (AFM-K, AFM-S, AKF-S) projections: Computers & Geosciences, v. 36, no. 6, p. 786–791, doi:10.1016/j.cageo.2010.01.001.

Galer, S., and Abouchami, W., 1998, Practical application of lead triple spiking for correction of instrumental mass discrimination: Mineralogical Magazine, v. 62A, p. 491–492, doi:10.1180/minmag.1998.62A.1.260.

Gannoun, A., Burton, K.W., Parkinson, I.J., Alard, O., Schiano, P., and Thomas, L.E., 2007, The scale and origin of the osmium isotope variations in mid-ocean ridge basalts: Earth and Planetary Science Letters, v. 259, no. 3–4, p. 541–556, doi:10.1016/j.epsl.2007.05.014.

Gazel, E., Hayes, J.L., Hoernle, K., Kelemen, P., Everson, E., Holbrook, W.S., Hauff, F., van den Bogaard, P., Vance, E.A., Chu, S., Calvert, A.J., Carr, M.J., and Yogodzinski, G.M., 2015, Continental crust generated in oceanic arcs: Nature Geoscience, v. 8, no. 4, p. 321–327, doi:10.1038/ngeo2392.

Ghiorso, M.S., and Gualda, G.A.R., 2015, An H_2O-CO_2 mixed fluid saturation model compatible with rhyolite-MELTS: Contributions to Mineralogy and Petrology, v. 169, no. 6, p. 1–30, doi:10.1007/s00410-015-1141-8.

Ghiorso, M.S., and Sack, R.O., 1995, Chemical mass transfer in magmatic processes IV. A revised and internally consistent thermodynamic model for the interpolation and extrapolation of liquid-solid equilibria in magmatic systems at elevated temperatures and pressures: Contributions to Mineralogy and Petrology, v. 119, no. 2, p. 197–212, doi:10.1007/BF00307281.

Ghiorso, M.S., Hirschmann, M.M., Reiners, P.W., and Kress, V.C., 2002, The pMELTS: A revision of MELTS for improved calculation of phase relations and major element partitioning related to partial melting of the mantle to 3 GPa: Geochemistry, Geophysics, Geosystems, v. 3, no. 5, p. 1–35, doi:10.1029/2001GC000217.

Global Volcanism Program, 2015, Report on Kick 'em Jenny (Grenada), *in* Sennert, S.K, ed., Weekly Volcanic Activity Report, 22 July–28 July 2015: Smithsonian Institution Global Volcanism Program and U.S. Geological Survey.

Graham, A.M., 1980, Genesis of the igneous rock suites of Grenada, Lesser Antilles [Ph.D. thesis]: University of Edinburgh, 337 p.

Grove, T., Elkins-Tanton, L., Parman, S., Chatterjee, N., Müntener, O., and Gaetani, G., 2003, Fractional crystallization and mantle-melting controls on calc-alkaline differentiation trends: Contributions to Mineralogy and Petrology, v. 145, no. 5, p. 515–533, doi:10.1007/s00410-003-0448-z.

Hawkesworth, C.J., and Powell, M., 1980, Magma genesis in the Lesser Antilles island arc: Earth and Planetary Science Letters, v. 51, no. 2, p. 297–308, doi:10.1016/0012-821X(80)90212-5.

Huang, F., Lundstrom, C.C., Sigurdsson, H., and Zhang, Z., 2011, U-series disequilibria in Kick'em Jenny submarine volcano lavas: A new view of time-scales of magmatism in convergent margins: Geochimica et Cosmochimica Acta, v. 75, no. 1, p. 195–212, doi:10.1016/j.gca.2010.05.036.

Kelemen, P.B., Hanghøj, K., and Greene, A.R., 2014, One view of the geochemistry of subduction-related magmatic arcs, with an emphasis on primitive andesite and lower crust, *in* Holland, H.D., and Turekian, K.K., eds., Treatise on Geochemistry (second edition): Oxford, Elsevier, Reference Module in Earth Systems and Environmental Sciences, v. 4, p. 749–806, doi:10.1016/B978-0-08-095975-7.00323-5.

Kessel, R., Schmidt, M.W., Ulmer, P., and Pettke, T., 2005, Trace element signature of subduction-zone fluids, melts and supercritical liquids at 120–180 km depth: Nature, v. 437, no. 7059, p. 724–727, doi:10.1038/nature03971.

Kuiper, K.F., Deino, A., Hilgen, F.J., Krijgsman, W., Renne, P.R., and Wijbrans, J.R., 2008, Synchronizing rock clocks of Earth history: Science, v. 320, no. 5875, p. 500–504, doi:10.1126/science.1154339.

Labanieh, S., Chauvel, C., Germa, A., Quidelleur, X., and Lewin, E., 2010, Isotopic hyperbolas constrain sources and processes under the Lesser Antilles arc: Earth and Planetary Science Letters, v. 298, no. 1–2, p. 35–46, doi:10.1016/j.epsl.2010.07.018.

Martin, L.A.J., Hermann, J., Gauthiez-Putallaz, L., Whitney, D.L., Brovarone, A.V., Fornash, K.F., and Evans, N.J., 2014, Lawsonite geochemistry and stability—Implication for trace element and water cycles in subduction zones: Journal of Metamorphic Geology, v. 32, no. 5, p. 455–478, doi:10.1111/jmg.12093.

McDonough, W.F., and Sun, S.S., 1995, The composition of the Earth: Chemical Geology, v. 120, no. 3–4, p. 223–253, doi:10.1016/0009-2541(94)00140-4.

Médard, E., Schmidt, M., and Schiano, P., 2004, Liquidus surfaces of ultracalcic primitive melts: Formation conditions and sources: Contributions to Mineralogy and Petrology, v. 148, no. 2, p. 201–215, doi:10.1007/s00410-004-0591-1.

Miyashiro, A., 1974, Volcanic rock series in island arcs and active continental margins: American Journal of Science, v. 274, no. 4, p. 321–355, doi:10.2475/ajs.274.4.321.

Nagle, F., Stipp, J.J., and Fisher, D.E., 1976, K-Ar geochronology of the Limestone Caribbees and Martinique, Lesser Antilles, West Indies: Earth and Planetary Science Letters, v. 29, no. 2, p. 401–412, doi:10.1016/0012-821X(76)90145-X.

O'Hara, M.J., 1968, The bearing of phase equilibria studies in synthetic and natural systems on the origin and evolution of basic and ultrabasic rocks: Earth-Science Reviews, v. 4, p. 69–133, doi:10.1016/0012-8252(68)90147-5.

Parkinson, I.J., Arculus, R.J., and Eggins, S.M., 2003, Peridotite xenoliths from Grenada, Lesser Antilles Island Arc: Contributions to Mineralogy and Petrology, v. 146, no. 2, p. 241–262, doi:10.1007/s00410-003-0500-z.

Pichavant, M., and Macdonald, R., 2007, Crystallization of primitive basaltic magmas at crustal pressures and genesis of the calc-alkaline igneous suite: Experimental evidence from St

Vincent, Lesser Antilles arc: Contributions to Mineralogy and Petrology, v. 154, no. 5, p. 535–558, doi:10.1007/s00410-007-0208-6.
Plank, T., 2014, The chemical composition of subducting sediments, *in* Turekian, K.K., and Holland, H.D., eds., Treatise on Geochemistry (second edition), Volume 4: Oxford, Elsevier, p. 607–629.
Plank, T., 2016, Subduction zone geochemistry, *in* White, W.M., ed., Encyclopedia of Geochemistry: A Comprehensive Reference Source on the Chemistry of the Earth: Cham, Springer International Publishing, p. 1–9, doi:10.1007/978-3-319-39193-9_268-1.
Reubi, O., Bourdon, B., Dungan, M.A., Koornneef, J.M., Sellés, D., Langmuir, C.H., and Aciego, S., 2011, Assimilation of the plutonic roots of the Andean arc controls variations in U-series disequilibria at Volcan Llaima, Chile: Earth and Planetary Science Letters, v. 303, no. 1–2, p. 37–47, doi:10.1016/j.epsl.2010.12.018.
Salters, V.J.M., and Stracke, A., 2004, Composition of the depleted mantle: Geochemistry, Geophysics, Geosystems, v. 5, no. 5, Q05B07, doi:10.1029/2003GC000597.
Schiano, P., Eiler, J.M., Hutcheon, I.D., and Stolper, E.M., 2000, Primitive CaO-rich, silica-undersaturated melts in island arcs: Evidence for the involvement of clinopyroxene-rich lithologies in the petrogenesis of arc magmas: Geochemistry, Geophysics, Geosystems, v. 1, no. 5, 1018, doi:10.1029/1999GC000032.
Schmidt, M.W., Vielzeuf, D., and Auzanneau, E., 2004, Melting and dissolution of subducting crust at high pressures: The key role of white mica: Earth and Planetary Science Letters, v. 228, no. 1–2, p. 65–84, doi:10.1016/j.epsl.2004.09.020.
Sigurdsson, H., and Shepherd, J.B., 1974, Amphibole-bearing basalts from the submarine volcano Kick'em-Jenny in the lesser Antilles Island arc: Bulletin Volcanologique, v. 38, no. 3, p. 891–910, doi:10.1007/BF02597097.
Sigurdsson, H., Tomblin, J.F., Brown, G.M., Holland, J.G., and Arculus, R.J., 1973, Strongly undersaturated magmas in the Lesser Antilles island arc: Earth and Planetary Science Letters, v. 18, no. 2, p. 285–295, doi:10.1016/0012-821X(73)90067-8.
Sorbadere, F., Schiano, P., and Metrich, N., 2012, Constraints on the origin of nepheline-normative primitive magmas in island arcs inferred from olivine-hosted melt inclusion compositions: Journal of Petrology, v. 54, p. 215–233.
Sorbadere, F., Médard, E., Laporte, D., and Schiano, P., 2013, Experimental melting of hydrous peridotite-pyroxenite mixed sources: Constraints on the genesis of silica-undersaturated magmas beneath volcanic arcs: Earth and Planetary Science Letters, v. 384, p. 42–56, doi:10.1016/j.epsl.2013.09.026.
Speed, R.C., and Walker, J.A., 1991, Oceanic crust of the Grenada Basin in the Southern Lesser Antilles Arc Platform: Journal of Geophysical Research. Solid Earth, v. 96, no. B3, p. 3835–3851, doi:10.1029/90JB02558.
Speed, R.C., Smith-Horowitz, P.L., Perch-Nielsen, K.S., Saunders, J.B., and Sanfilippo, A.B., eds., 1993, Southern Lesser Antilles Arc Platform: Pre-Late Miocene Stratigraphy, Structure, and Tectonic Evolution: Geological Society of America Special Paper 277, 98 p.
Stamper, C.C., Blundy, J.D., Arculus, R.J., and Melekhova, E., 2014a, Petrology of plutonic xenoliths and volcanic rocks from Grenada, Lesser Antilles: Journal of Petrology, v. 55, no. 7, p. 1353–1387, doi:10.1093/petrology/egu027.
Stamper, C.C., Melekhova, E., Blundy, J.D., Arculus, R.J., Humphreys, M.C.S., and Brooker, R.A., 2014b, Oxidised phase relations of a primitive basalt from Grenada, Lesser Antilles: Contributions to Mineralogy and Petrology, v. 167, no. 1, p. 1–20, doi:10.1007/s00410-013-0954-6.
Syracuse, E.M., van Keken, P.E., and Abers, G.A., 2010, The global range of subduction zone thermal models: Physics of the Earth and Planetary Interiors, v. 183, no. 1–2, p. 73–90, doi:10.1016/j.pepi.2010.02.004.
Tatsumi, Y., and Kogiso, T., 2003, The subduction factory: Its role in the evolution of the Earth's crust and mantle, *in* Larter, R.D., and Leat, P.T., eds., Intra-Oceanic Subduction Systems: Tectonic and Magmatic Processes: Geological Society of London Special Publication 219, no. 1, p. 55–80, doi:10.1144/GSL.SP.2003.219.01.03.
Taylor, S.R., and McLennan, S.M., 1985, The Continental Crust: Its Composition and Evolution: Oxford, Blackwell Scientific Publications, 312 p.
Thirlwall, M.F., and Graham, A.M., 1984, Evolution of high-Ca, high-Sr C-series basalts from Grenada, Lesser Antilles: The effects of intra-crustal contamination: Journal of the Geological Society of London, v. 141, no. 3, p. 427–445.
Thirlwall, M.F., Graham, A.M., Arculus, R.J., Harmon, R.S., and Macpherson, C.G., 1996, Resolution of the effects of crustal assimilation, sediment subduction, and fluid transport in island arc magmas; Pb-Sr-Nd-O isotope geochemistry of Grenada, Lesser Antilles: Geochimica et Cosmochimica Acta, v. 60, no. 23, p. 4785–4810, doi:10.1016/S0016-7037(96)00272-4.
Thirlwall, M.F., Smith, T.E., Graham, A.M., Theodorou, N., Hollings, P., Davidson, J.P., and Arculus, R.J., 1994, High field strength element anomalies in arc lavas: Source or process?: Journal of Petrology, v. 35, no. 3, p. 819–838, doi:10.1093/petrology/35.3.819.
Turner, S., Hawkesworth, C., van Calsteren, P., Heath, E., Macdonald, R., and Black, S., 1996, U-series isotopes and destructive plate margin magma genesis in the Lesser Antilles: Earth and Planetary Science Letters, v. 142, no. 1–2, p. 191–207, doi:10.1016/0012-821X(96)00078-7.
Turner, S., Evans, P., and Hawkesworth, C., 2001, Ultrafast source-to-surface movement of melt at island arcs from ^{226}Ra-^{230}Th systematics: Science, v. 292, no. 5520, p. 1363–1366, doi:10.1126/science.1059904.
Watlington, R.A., Wilson, W.D., Johns, W.E., and Nelson, C., 2002, Updated bathymetric survey of Kick-'em-Jenny submarine volcano: Marine Geophysical Researches, v. 23, no. 3, p. 271–276, doi:10.1023/A:1023615529336.
Westercamp, D., 1988, Magma generation in the Lesser Antilles: Geological constraints: Tectonophysics, v. 149, no. 1, p. 145–163, doi:10.1016/0040-1951(88)90123-0.
Westercamp, D., Andreieff, P., Bouysse, P., Mascale, A., and Baubron, J.C., 1985, The Grenadines, southern Lesser Antilles: Part 1—Stratigraphy and volcano-structural evolution: Paris, Géodynamique de Caraibes Symposium, *in* Mascale, A., ed., Editions Technip, p. 109–118.
White, W.M., and Dupré, B., 1986, Sediment subduction and magma genesis in the Lesser Antilles: Isotopic and trace element constraints: Journal of Geophysical Research, v. 91, p. 5927–5941, doi:10.1029/JB091iB06p05927.
White, W.M., and Klein, E.M., 2014, 4.13: Composition of the oceanic crust, *in* Holland, H.D., and Turekian, K.K., eds., Treatise on Geochemistry (second edition): Oxford, Elsevier, p. 457–496, doi:10.1016/B978-0-08-095975-7.00315-6.
White, W.M., and Patchett, J., 1984, Hf-Nd-Sr isotopes and incompatible element abundances in island arcs: Implications for magma origins and crust-mantle evolution: Earth and Planetary Science Letters, v. 67, no. 2, p. 167–185, doi:10.1016/0012-821X(84)90112-2.
White, W.M., Dupré, B., and Vidal, P., 1985, Isotope and trace element geochemistry of sediments from the Barbados Ridge–Demerara Plain region, Atlantic Ocean: Geochimica et Cosmochimica Acta, v. 49, no. 9, p. 1875–1886, doi:10.1016/0016-7037(85)90082-1.
Woodland, S.J., Pearson, D.G., and Thirlwall, M.F., 2002, A platinum group element and Re-Os isotope investigation of siderophile element recycling in subduction zones: Comparison of Grenada, Lesser Antilles Arc, and the Izu-Bonin Arc: Journal of Petrology, v. 43, no. 1, p. 171–198, doi:10.1093/petrology/43.1.171.
Zack, T., Foley, S.F., and Jenner, G.A., 1997, A consistent partition coefficient set for clinopyroxene, amphibole and garnet from laser ablation microprobe analysis of garnet pyroxenites from Kakanui, New Zealand: Neues Jahrbuch für Mineralogie (Abhandlungen), v. 172, p. 23–41.